Published in final edited form as:

Structure. 2022 February 03; 30(2): 289–299.e6. doi:10.1016/j.str.2021.09.006.

Tsg101/ESCRT-I Recruitment Regulated by the Dual Binding Modes of K63-Linked Diubiquitin

Madeleine Strickland[1,#], **Susan Watanabe**[2,#], **Steven M. Bonn**[3], **Christina M. Camara**[3], **Mary R. Starich**[1], **David Fushman**[3], **Carol A. Carter**[2,*], **Nico Tjandra**[1,*]

[1]Biochemistry and Biophysics Center, National Heart, Lung, and Blood Institute, National Institutes of Health, Bethesda, MD, 20892, USA.

[2]Department of Microbiology & Immunology, Renaissance School of Medicine, Stony Brook University, Stony Brook, NY 11794-5222, USA.

[3]Department of Chemistry and Biochemistry, Center for Biomolecular Structure and Organization, University of Maryland, College Park, MD 20742, USA.

SUMMARY

The ESCRT-I protein Tsg101 plays a critical role in viral budding and endocytic sorting. Although Tsg101 is known to recognize monoubiquitin (Ub_1), here we show that it can also bind several diubiquitins (K48-Ub_2, N-Ub_2, and K63-Ub_2), with a preference for K63-linked Ub_2. The NMR structure of the Tsg101:K63-Ub_2 complex showed that while the Ub_1-binding site accommodates the distal domain of Ub_2, the proximal domain alternatively binds two different sites, the vestigial active site and an N-terminal helix. Mutation of each site results in distinct phenotypes regarding the recruitment of Tsg101 partners. Mutation in the vestigial active site abrogates interaction between Tsg101 and the HIV-1 protein Gag but not Hrs, a cellular protein. Mutation at the N-terminal helix alters Gag but not Hrs-Tsg101 localization. Given the broad involvement of Tsg101 in diverse cellular functions, this discovery advances our understanding of how the ESCRT protein recognizes binding partners and sorts endocytic cargo.

[*]Co-Corresponding Authors: Carol A. Carter, Department of Microbiology & Immunology, Stony Brook University, Life Sciences Bldg. Room 248, Stony Brook NY 11794-5222, USA, Telephone: (631) 632-8801, Telefax: (631) 632-9797, carol.carter@stonybrook.edu, Nico Tjandra (Lead Contact), Biochemistry and Biophysics Center, National Heart, Lung, and Blood Institute, 50 South Drive, Room 3503, Bethesda, MD 20892, USA, Telephone: (301) 402-3029, Telefax: (301) 402-3405, tjandran@nhlbi.nih.gov.

Author contributions are: M.S. conducted NMR structural analysis, wrote the paper; S.W. conducted Western analysis, fluorescence imaging studies and yeast 2-hybrid assays, wrote the paper; S.B. and C.M.C. made K48- and K63-linked Ub_2 and Ub_3 constructs; D.F. supervised and coordinated assembly of Ub chains and participated in paper writing; N.T. supervised structural analysis and overall project development; M.R.S performed chemical shift titrations, determined dissociation constants for ^{15}N-labeled Tsg101 bound to monoubiquitin and verified PTAP binding to Tsg101 mutants by NMR. C.A.C. supervised genetic, biochemical, and cell-biological analyses, coordinated structural and cell-based studies and project development, wrote the paper.

[#]These authors contributed equally

Declaration of Interests

M.S., N.T., and C.A.C. are co-inventors on a patent application which includes subject matter from this manuscript. The remaining authors declare no competing financial interests.

Graphical Abstract

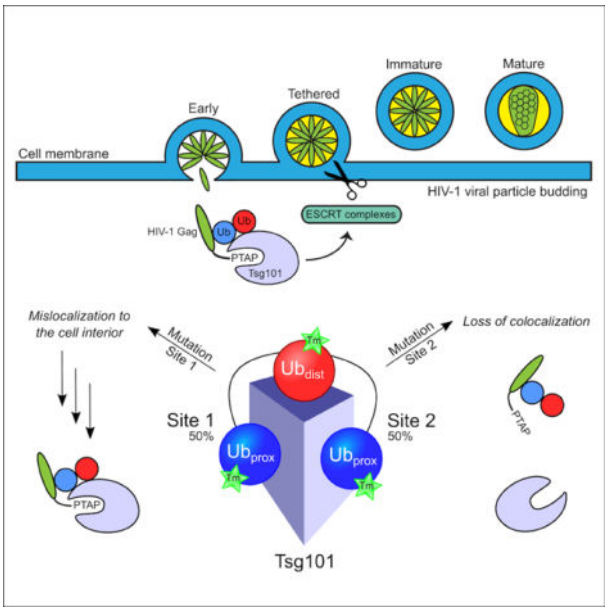

eTOC blurb

Strickland et al. determine the structure of the K63 linked Di-Ubiquitin bound to Tsg101 UEV domain. The structure reveals the distal Ubiquitin binds the mono-Ubiquitin site on UEV, whereas the proximal Ubiquitin can occupy two distinct sites. The two conformations of the Di-Ub on UEV have different functional consequences.

Keywords

ESCRT; Diubiquitin; Tsg101; Hrs; NMR; CPMG; viral budding; endocytic sorting

INTRODUCTION

Much is now known about how the *e*ndosomal *s*orting *c*omplexes *r*equired for *t*ransport (ESCRT-0, -I, -II, and -III) function to recognize internalized ubiquitinylated receptors, such as EGFR (epidermal growth factor receptor), transport them to the multivesicular body (MVB) for sorting, and ultimately deliver the cargo to degradative compartments in the cell interior (Baldys and Raymond, 2009; Kim et al., 2007; Lu et al., 2003) (reviewed in(Critchley et al., 2018)). Great strides have also been made towards understanding the mechanism underlying the membrane scission events mediated by ESCRT-III and Vps4 that result in MVB formation (Adell et al., 2014; Hanson and Cashikar, 2012). The canonical signal for cargo inclusion into an intraluminal vesicle of the MVB is covalent modification with ubiquitin (Ub), where Ub chains longer than four earmark the cargo for a degradation pathway. It is now recognized that the proteasome also accepts different Ub chain types (Clague and Urbe, 2010). Sequestration into a different MVB microdomain, as occurs following constitutive EGFR recycling, avoids budding into the lumen of the endosome (Eyster et al., 2011; Leonard et al., 2008). Many enveloped viruses exploit the

ESCRT-III complex for viral bud separation from the cell periphery (reviewed in refs. (Ahmed et al., 2019; Votteler and Sundquist, 2013)). However, beyond recognition that P(T/S)AP motifs in viral structural proteins permit them to recruit the Tsg101 protein and, thereby ESCRT-I, directly to viral assembly sites to serve as conduit to ESCRT-III (Garrus et al., 2001; Martin-Serrano et al., 2001; VerPlank et al., 2001), we lack a fundamental understanding of how Tsg101 functions in partner selection, sorting, and traffic routing. Based on observations that several of the early, but not late, functioning ESCRT-0, -I, and -II factors possess Ub-binding motifs, it is speculated that Ub modification might permit dynamic scaffolding of the ESCRT machinery and/or serve to concentrate Ub-modified cargoes into particular endosomal microdomains (Alam et al., 2004; Bilodeau et al., 2002; Gruenberg and Stenmark, 2004; Hurley, 2008; Katzmann et al., 2001; Piper and Luzio, 2007; Shih et al., 2002; Slagsvold et al., 2005).

The Ub-binding site in Tsg101 is housed in an N-terminal Ub E2 variant (UEV) domain with homology to the Ub-conjugating (Ubc) 4 subgroup of E2 enzymes (Koonin and Abagyan, 1997; Ponting et al., 1997). In canonical E2 enzymes, Ub is conjugated to an active-site Cys residue. In Tsg101 and its orthologues in plants to mammals, tyrosine replaces this residue and thus the protein is enzymatically inactive. This conserved unique feature of the Tsg101 protein has led to the speculation that Tsg101 might function as a dominant-negative interfering E2 that prevents or limits Ub modification and thereby influences partner destination. Of the many Tsg101-partner interactions identified to date, the Gag-Tsg101 interaction may exhibit the highest affinity (Pornillos et al., 2003). Furthermore, there is a direct correlation between the binding affinity and the ability of Tsg101 to support the release of infectious HIV-1 (Sharma et al., 2018), indicating that Tsg101-PTAP binding activity is essential for HIV-1 release. Nevertheless, we reported several years ago that mutation of the vestigial active site residue Y110 in human Tsg101, present in place of the active-site Cys that forms a thioester bond with Ub in the canonical E2 enzyme, impaired the Gag-Tsg101 interaction (VerPlank et al., 2001). We did not have a clear explanation for this observation, but hypothesized that determinants outside the P(T/S)AP-binding pocket can impact Gag-Tsg101 interaction. Here, we identify binding sites in the Tsg101 UEV domain for diubiquitin (Ub_2), a signaling molecule linked to diverse regulatory activities. Using NMR spectroscopy, Ub_2 molecules of three linkage types were assayed for binding to Tsg101; K63-linked Ub_2 was preferred. Due to the low affinity of the Tsg101:K63-Ub_2 complex, non-conventional NMR approaches were employed to determine the structure. The structure of the Tsg101:K63-Ub_2 complex that we solved revealed that the distal Ub of K63-linked Ub_2 localized in the previously identified Ub_1 binding site. Remarkably, the proximal Ub was located either close to the vestigial active site or a region near the N-terminal helix-1 and rapidly exchanged between the two sites. Guided by our structure, we designed UEV mutations in the distal or proximal Ub binding sites and tested their impact on P(T/S)AP-mediated Tsg101 binding to two unrelated and functionally distinct partners, the HIV-1 structural precursor protein, Gag, and the cellular ESCRT-0 component, *h*epatocyte growth factor-*r*egulated tyrosine kinase *s*ubstrate (Hrs). Interestingly we obtained different outcomes of proximal Ub binding site mutations. In vitro, we observed that Ala substitution of the Ub_2 proximal domain binding determinants located near the vestigial active site inhibited Gag-Tsg101 interaction, as previously seen for

P(T/S)AP binding site mutations (VerPlank et al., 2001). In contrast, Hrs-Tsg101 interaction appeared undisturbed. Mutation of determinants near the N-terminus had no inhibitory effect on the Gag- or Hrs-Tsg101 interaction but affected Gag-Tsg101 recruitment to the plasma membrane. We found that the Tsg101 P(T/S)AP binding site and the vestigial active site, even though they are spatially distinct, are coupled dynamically. This explains why mutations at either of these sites lead to inhibition of Gag-Tsg101 interaction. These findings suggest that Ub_2 might function independently or in conjunction with P(T/S)AP interaction in sorting of the Tsg101-partner complex to specific subcellular destinations. Overall, the results indicate that the P(T/S)AP motif alone is insufficient for Tsg101 recruitment and Ub_2 binding is needed to "fine-tune" Tsg101 control of the interaction.

RESULTS

Tsg101 preferentially binds to K63-Ub_2

We confirmed that Tsg101 binds to Ub_1 (Pornillos et al., 2002). We estimated the binding affinity by fitting the Tsg101 chemical shift changes observed by adding Ub_1. Representative binding curves obtained from ^{1}H and ^{15}N chemical shift changes are shown in Supplementary Figures 1 and 2, respectively. The fitted dissociation constants from those curves are summarized in Supplementary Table 1 with an average K_D ~800μM, which is relatively weak for Ub_1 interaction with Tsg101. However, until now, it was not clear whether Tsg101 is capable of binding to Ub chains. Since the Tsg101 UEV domain has recently been shown to contain a second, adjacent, ultra-low affinity binding site for Ub (Mishra et al., 2018), we proposed that Tsg101 may have the capacity to bind polyubiquitin (poly-Ub) chains. Poly-Ub chains are formed when the C-terminal carboxy group of one Ub molecule is connected via an isopeptide bond to a side-chain ε-amino group in any of the seven lysines in a second Ub molecule, or via a peptide bond to the N-terminal amine. We chose to investigate three different Ub_2 molecules – two with an isopeptide linkage (K48-Ub_2 and K63-Ub_2), and one with a "linear" peptide linkage (N-Ub_2). NMR chemical shift perturbations (CSPs) were used to assay the nature and location of Ub_2 binding to Tsg101 in comparison to the Ub_1 binding site, which was studied previously (Pornillos et al., 2002; Strickland et al., 2017; Sundquist et al., 2004; Teo et al., 2004) (Fig. 1a–d). Interestingly, all three Ub_2 molecules perturbed the known Ub_1 binding site (including group 1 residues L39, V43, D46, G47, C87, V89, T92, N106, G107 – gray shading in Fig. 1a–d) as well as residues outside of that site (group 2 residues V28, H111, H115, H119, L124, G126 – yellow shading in Fig. 1a–d). All three diubiquitin molecules induced a similar set of CSPs in Tsg101, indicating that they had similar binding modes (Fig. 1e–h). However, there were some differences in the strength of those CSPs in the Ub_1 binding site (shaded grey in Fig. 1a–d, Supplementary Fig. 3). The average CSP for group 1 residues in Tsg101 was the strongest upon addition of K63-Ub_2 (0.032 ppm), followed by Ub_1 (0.023 ppm), N-Ub_2 (0.020 ppm), and K48-Ub_2 (0.015 ppm). The variations of chemical shift changes can be seen from the overlay of NMR spectra of ^{15}N-Tsg101 with and without the presence of Ub_1, K48-Ub_2, N-Ub_2, and K63-Ub_2 in Supplementary Fig 4a, b, c, and d, respectively. This led us to conclude that Tsg101 has a slight preference for K63-Ub_2

Both ubiquitin units of K63-Ub_2 bind to Tsg101 using the canonical I44 hydrophobic patch

Since blocking the interaction of Tsg101 and Ub_1 leads to broad-spectrum antiviral activity (Strickland et al., 2017) and Watanabe et al., 2020), we strove to characterize the structural basis for Tsg101-Ub_2 recognition, as this could constitute a new target for viral budding inhibitors. Using NMR spectroscopy, we set out to determine the Tsg101:K63-Ub_2 structure starting with the crystal structures of Tsg101 (Sundquist et al., 2004) and K63-Ub_2 (Weeks et al., 2009) with the chemical shift perturbations as a structural restraint to determine the location of the interface. However, Ub_2 is difficult to study by NMR, given that the chemical shifts of both the distal and the proximal Ubs are virtually identical and lead to severe overlap in the NMR spectra. To deal with this, we measured the CSPs for K63-Ub_2 using two samples – each with one of the Ub units labeled with ^{15}N and the other at natural abundance. Each Ub was expressed and labeled appropriately in *E. coli*, purified, and then linked enzymatically, as described previously (Pickart and Raasi, 2005; Varadan et al., 2005; Varadan et al., 2004; Varadan et al., 2002). Interestingly, both Ub units underwent very similar CSPs upon addition of unlabeled Tsg101, each using the canonical hydrophobic surface patch centered on ubiquitin residue I44 (Supplementary Fig. 5a). Large CSPs were plotted on the surface of K63-Ub_2 (PDB: 3H7P (Weeks et al., 2009), Supplementary Fig. 5b), confirming that both Ubs were using the same interface.

The distal ubiquitin of K63-Ub_2 binds to Tsg101 in the same location as Ub_1

Although the CSPs could be used as a restraint in the structure calculation of Tsg101 and K63-Ub_2, additional restraints were required to ascertain the orientation of the two molecules with respect to each other. Since the affinity between Tsg101 and Ub in general is relatively weak, we chose to use a non-NOE based NMR distance measurement. Lanthanide tags can induce pseudocontact shifts (PCSs) in residues up to 56 Å away in a distance- and angle-dependent manner (Keizers et al., 2010). By attaching a lanthanide tag (Tm-DOTA-M8-SPy) to each Ub unit in Ub_2 individually, we could determine where each Ub contacts ^{15}N-Tsg101, as well as their relative orientation in the complex. As a control we measured Tsg101 amide proton PCSs induced by Tm-M8-Ub_1^{T14C} (Fig. 2a, black circles) and fit them to the known crystal structure of the Tsg101: Ub_1 complex (Sundquist et al., 2004) (PDB ID: 1S1Q; Figure 2a, black lines). *Q*-factors were used to assay the quality of the fit between PCSs and the structure, where a lower number indicates a better fit (Cornilescu et al., 1998; Strickland and Tjandra, 2018). The fit between the Tsg101:Ub_1 structure and the measured PCSs was excellent, as indicated by the *Q*-factor of 24.6% (Fig. 2d). Tsg101 PCSs were then measured in complex with Tm-M8-K63-Ub_2 conjugated at the mutated T14C residue in the distal (Fig. 2b,e) or proximal (Fig. 2c,f) Ub unit. Interestingly, the distal Ub of K63-Ub_2 binds in the same position and orientation as Ub_1, as indicated by the similarity between the measured PCSs (Fig. 2a,b). This meant that Tsg101 and the distal Ub could be held fixed to the Ub_1:Tsg101 crystal structure coordinates throughout the structure calculation, decreasing the large number of conformational possibilities and thereby increasing the efficiency of the calculations.

The CSPs and PCS data sets were used as restraints, in addition to other non-bonded potentials (see Materials and Methods), to calculate the structure of the Tsg101:K63-Ub_2 complex using the simulated annealing protocol of Xplor-NIH (Schwieters et al.,

2006; Schwieters et al., 2003). Although the distal Ub PCSs fit well to the Tsg101:Ub_1 structure, no single position could accurately describe the Tsg101 PCSs measured for the tagged proximal Ub. Restraining the structure calculation to a single proximal Ub binding conformation results in poor agreement to the measured PCS values (Supplementary Fig 6a–e). However, two clusters of structures were found that could satisfy the PCS restraints when combined. Using the lowest energy structures from each cluster as input for a refinement with two ensemble members, PCSs could be satisfied for both the distal (Q=31.7%) and proximal (Q=33.0%) Ubs, as shown in Fig. 2e,f.

Structure of the Tsg101:K63-Ub_2 complex

The lowest energy structural ensemble of Tsg101:K63-Ub_2 is shown in Fig. 3 (PDB ID: 6UD0, BMRB ID: 30675, Table 1). Fig. 3 compares the two members of the ensemble. Although the distal Ub is located in the same orientation and location as Ub_1 (Sundquist et al., 2004) in both structures, the proximal Ub shares its time between two locations – one near the N-terminal α-helix of Tsg101, and one close to the vestigial Ub-binding site. The core structure of the UEV domain of Tsg101 consists of a twisted β-sheet, with the first two strands elongated in a β-hairpin. The β-hairpin contacts all three ubiquitin binding sites, with the inside face contacting the distal Ub, and the outside face and side contacting the proximal Ub in sites 1 and 2, respectively (Fig. 3). Although all three Tsg101 Ub-binding sites have very different overall folds, Ub residues I44, A46, H68 are involved in binding to the Tsg101 in all three sites.

K63-Ub_2 binding determinants modulate Gag p6-domain PTAP-interaction

The structural model was used to guide mutagenesis experiments aimed at evaluating the impact that Ub_2 binding might have on Tsg101 recruitment by Gag or Hrs. To rule out the possibility of the mutations altering the structure of Tsg101 significantly we compared the ^{1}H-^{15}N HSQC spectra of the wildtype protein against its mutants that showed significant change in their Gag interaction (Supplementary Fig. 7a–c). The NMR spectra confirm that the mutations only induce local structural changes while still preserving the overall fold of Tsg101. Furthermore, these mutations do not affect those residues responsible for P(T/S)AP recognition (Supplementary Fig. 7a–c), or the ability of Tsg101 to bind P(T/S)AP derived peptide (Supplementary Fig. 7d–f). Using yeast two hybrid assay we evaluated the impact of mutations on Tsg101 for Gag binding specifically. Mutation of determinants of the Ub_2 distal Ub binding located at the β-hairpin did not inhibit Gag-Tsg101 interaction, whether examined in the context of p6 domain alone or full-length Gag (Fig. 4a). This is in agreement with our previous studies, which demonstrated that disruption of Ub binding at the β-hairpin site by a small molecule did not prevent the PTAP interaction at the P(T/S)AP-binding pocket (Strickland et al., 2017). Similarly, mutation of determinants of Ub_2 proximal Ub binding at the N-terminal helix location also did not inhibit Gag-Tsg101 interaction. Indeed, several of the mutations promoted interaction, as does PTAP duplication. By contrast, mutation of determinants of Ub_2 binding near the vestigial active site blocked Gag-Tsg101 interaction, eventhough as stated above, this mutation does not affect PTAP binding. Thus, the two Ub_2 binding modes had opposite impact on Gag-Tsg101 interaction, raising the possibility that they differentially influenced PTAP binding pocket accessibility. In particular, it was rather puzzling how mutations in the Tsg101 P(T/S)AP binding pocket

or the vestigial active site could have the same outcome (inhibiting Gag interaction), since these sites are distinct (Fig. 4b). We posited that these two sites must be somehow linked, despite their spatial separation. We examined this possibility using NMR experiments that are sensitive to conformational changes, ligand binding, and dynamics.

Using CSPs, it was previously shown that tenatoprazole, a covalent Tsg101-Ub_1 inhibitor engaging C73, did not affect the binding of a Gag p6-mimicking peptide to Tsg101, indicating that PTAP and Ub_1 binding could occur independently (Strickland et al., 2017). Although CSPs can provide information on ligand binding and changes in average structure, they are insensitive to changes in dynamics. We used NMR CPMG experiments to investigate the dynamics of PTAP binding (Fig. 5). Natural abundance PTAP peptide was added into a 300 μM solution of ^{15}N-Tsg101 at a 1:1 ratio. Fig. 5a shows the change in ^{15}N R_2 relaxation rate observed at two different τ_{cp} values. Residues with large changes are highlighted in blue and are considered to be undergoing significant dynamics on the μs-ms time-scale. Since no large changes are observed for the free form of Tsg101 (Fig. 5b), residues highlighted in Fig. 5a can be attributed to changes in dynamics upon ligand binding. PTAP binding induces changes around the PTAP binding site (Fig. 5c) as expected, along with four residues in the second binding site of the proximal Ub of K63-Ub_2 (N83, L114, W116, K118) (Fig. 5d). By contrast, the binding site of the distal Ub of K63-Ub_2 (or indeed Ub_1) underwent no significant changes in dynamics (Fig. 5d). The results indicate that there is indeed dynamic coupling between the PTAP binding site and the K63-Ub_2 binding at the vestigial active site of Tsg101 consistent with the observed inhibition of Gag-Tsg101 binding following mutation of either the PTAP binding site or the vestigial active site region.

UEV determinants that modulate Gag p6-P(T/S)AP-interaction impact Gag- but not Hrs-Tsg101 co-localization.

It is well-established that Gag recruits Tsg101 to budding sites at the cell periphery by engaging the UEV PTAP-binding pocket (Garrus et al., 2001; Martin-Serrano et al., 2001; VerPlank et al., 2001). Finding that disruption of determinants of Ub_2 binding near the vestigial active site abrogated direct Tsg101 interaction with Gag, as measured by the yeast 2-hybrid assay (Fig. 4), despite the presence of an intact PTAP-binding pocket in the Tsg101 protein suggests that a dynamic competition or cooperation exist between the Ub_2 and PTAP binding sites in Gag. This notion is supported by the results above (Fig. 5). We examined the effect of mutation of the Ub_2-binding determinants in cells co-expressing Gag or Hrs and mutated Tsg101 proteins. As shown in Fig. 6a, WT Tsg101 (red signal) co-expressed with WT Gag (green signal) accumulated at the cell periphery, as indicated by the yellow signal in the merged red and green images. This is as expected based on previous observations from our laboratory and others (Goff et al., 2003; Strickland et al., 2017). Also as expected based on previous studies, disruption of the PTAP sequence in Gag (P7L, Fig. 6b) or the P(T/S)AP-binding pocket in Tsg101 (M95A, Fig. 6c) prevented or interfered with this co-localization, respectively (Goff et al., 2003; Strickland et al., 2017). These findings are consistent with the conclusion that the PTAP motif in Gag mediates the delivery of Tsg101 to Gag assembly sites on the plasma membrane. Interference with the N-terminal determinants important for recognition of the Ub_2 proximal Ub unit (KK9,10AA) did not prevent Gag-Tsg101 co-localization at the plasma membrane. However, this disruption

resulted in sequestration of a subpopulation of Gag and Tsg101 in the perinuclear region (Fig. 6d). In contrast, although the Ub_2 distal Ub binding site Y42A-Tsg101 mutant retained the ability to bind Gag in vitro (Fig. 4), it was less able to recruit Tsg101 to the periphery (Fig. 6e). Consistent with the conclusion that the determinants of Ub_2 binding at the vestigial active site dominate PTAP recognition, disruption of the vestigial active site by substitution of Ala for Y110 (Fig. 6f) reduced Gag-Tsg101 co-localization in cells. In contrast, mutations to disrupt N-terminal proximal Ub (KK9,10AA), distal Ub (Δ41–43), or proximal vestigial active site Ub interaction failed to prevent Hrs recruitment by Tsg101 (Fig. 6k, l, and m, respectively) which, like Gag, depends on UEV determinants (Fig. 6i) including P(T/S)AP recognition (Fig. 6j). Taken together, these observations indicate (i) that despite the existence of an intact PTAP-binding pocket, engaging Gag and being recruited by Gag are independent functions and (ii), that residues within Tsg101 distinguish these events. Fig. 6g and 6n show the range of Pearson's coefficients of correlation normalized to WT values. Collectively, the results indicate that disruption of the Ub_2 binding sites impacted the ability of Gag to recruit Tsg101 to the plasma membrane, while they had no apparent effect on Hrs interaction.

DISCUSSION

Tsg101 is known to facilitate the sorting and delivery of endocytic cargo to various cell destinations (reviewed in refs. (Ahmed et al., 2019; Frankel and Audhya, 2018)). A key structural determinant of its ability to conduct this function is a P(T/S)AP-binding pocket in its N-terminal UEV domain that engages the PSAP motif in Hrs/ESCRT-0, bringing the ESCRT-I complex to the early endosome (Lu et al., 2003). Gag mimics Hrs in using a P(T/S)AP motif to recruit Tsg101 to virus assembly sites on the plasma membrane (Pornillos et al., 2003). Disruption of the PTAP motif in HIV-1 Gag (e.g., a mutant encoding L_7TAP in lieu of PTAP, P7L-Gag) inhibits Tsg101/ESCRT-I engagement and the consequent recruitment of the membrane scission machinery housed in ESCRT-III, resulting in accumulation of virus-like particles (VLPs) with unsevered bud necks with a canonical "lollipop" appearance (Gottlinger et al., 1991). Treatments that interfere with recruitment of the membrane scission machinery housed in ESCRT-III have an identical impact, identifying the cause of the defect as a failure to engage this complex. The PTAP motif is thus considered as the mediator of a late-acting (L) domain in Gag (Wills and Craven, 1991). Previous studies linked engagement of Ub conjugation machinery to the L domain function in retrovirus release (Strack et al., 2000) (reviewed in refs. (Carter, 2002; Vogt, 2000)) and demonstrated that interference with Ub removal from Gag is deleterious to particle release (Sette et al., 2013). The precise role of mono, di-, poly and linkage-specific Ub signaling in endosomal trafficking in the cell is still unclear. Tsg101 plays a critical part, not only in recognition of Ub-modified cargo destined for delivery to degradative compartments in the cell interior, but also in constitutive cargo trafficking to the cell periphery (Eyster et al 2011; Strickland 2017). We previously demonstrated constitutive cargo recycling to the plasma membrane, Gag-mediated recruitment of Tsg101 to the cell periphery and consequently, viral budding (Strickland et al., 2017) as well as with EBV-directed trafficking to the periphery of viral capsids assembled in the nucleus following activation from latency (Mannemuddhu et al 2021). Determinants in the Tsg101 UEV domain that recognize nucleic

acid (Watanabe et al 2020) overlap with some of those identified here as important for Ub_2 binding (reviewed in Strickland 2021), suggesting that the protein possesses a broad range of potentially regulating modifiers.. Our current structural study was aimed at better understanding of the role of Ub signaling in Tsg101 function and has led to four important findings:

i) Using NMR to monitor molecular interaction, we showed that Tsg101 not only recognizes Ub_1, as previously reported, (Pornillos et al., 2002; Sundquist et al., 2004; Teo et al., 2004) but also several forms of Ub_2, of which the K63-linked Ub_2 interaction was slightly favored.

ii) In the complex with Tsg101, K63-linked Ub_2 surprisingly adopts two different conformations, where the distal Ub binds in the Ub_1 binding site, while the proximal Ub can bind equally well either to the site near the N-terminal helix (site 1) or at the Tsg101 vestigial active site (site 2). Our NMR data does not unequivocally rule out the possibility of a small population of a reversed conformation, wherein the proximal Ub domain binds the Ub_1 site and the distal binds at the other two sites.

iii) We showed that the determinants of Ub_2 proximal Ub binding at site 2 (vestigial active site) also specify Tsg101 recognition of HIV-1 Gag. This provides an explanation for our earlier finding that mutation of the vestigial active site and proximal residues abrogated Gag interaction despite the intact P(T/S)AP-binding pocket in Tsg101 and L domain in Gag p6(VerPlank et al., 2001). Thus, disruption of the P(T/S)AP-binding pocket or disruption of the vestigial active site is sufficient to prevent Gag (or p6) interaction with Tsg101. This finding suggests that P(T/S)AP motif recognition by the Tsg101 P(T/S)AP-binding pocket is directly coupled to Ub_2 binding at the vestigial site. We further identified using NMR CPMG analysis that the P(T/S)AP binding pocket and the vestigial active site are coupled dynamically, eventhough they are spatially distinct.

iv) We observed no inhibition of Gag-Tsg101 interaction following interference with the Ub_2 proximal Ub binding site 1 determinants (located near the UEV N-terminus). Rather, mutation of these determinants reproducibly increased signaling generated by Gag-Tsg101 interaction in the in an vitro assay (*c.f.*, Fig 4). In a cellular assay, the mutations resulted in increased Tsg101 or Tsg101/Gag signal intensity in the cell interior (*c.f.*, Fig. 6). This finding indicates mis-trafficking of the complex and suggests that dynamic site occupancy is a regulating component of the K63-Ub_2 function.

Through its structural homology to Ub E2 conjugases and UEV proteins, the vestigial active site region could permit Tsg101 to associate with the catalytic domain of E3 ligases. Indeed, we previously reported co-immunoprecipitation of Tsg101 and a member of the Nedd4 family of Ub E3 ligases in cells expressing HIV-1 Gag (Medina et al., 2005). In this regard, it should be noted that Sundquist and colleagues demonstrated that the stimulation of HIV-1 PTAP release by the E3 ligase Nedd4-2s depends on Tsg101/ESCRT-I (Chung et al., 2008). Curiously, they reported that the Ub-binding activity of Tsg101 was not required for the rescue of HIV-1 budding by Nedd4-2s, which they tested by mutation of the β-hairpin. We observed that mutation of the β-hairpin did not disrupt Gag-Tsg101 interaction in vitro (Fig. 4a) although we found that it interfered with their co-localization in cells expressing the

two proteins (Fig. 6). Possibly, these variations reflect differences in occupancy of the distal Ub of Ub_2 compared to the Ub_1 binding site. The potential ability of specific Ub-binding determinants in the Tsg101 protein to influence binding partner recognition suggests that the mechanism underlying the sorting decisions that determine whether a protein enters the MVB lumen or is delivered intact to the plasma membrane lies in control of the degree and form of Ub modification that the Tsg101 binding partner is permitted to receive from ligases in the interaction environment. It is interesting to note that the ESCRT-0 factor STAM recognizes K63-linked Ub_2 and employs it to stabilize association with a deubiquitinating enzyme (DUB) (Kim et al., 2006; McCullough et al., 2006). Ub and DUb are important co-factors in MVB formation, constitutive trafficking (Eyster 2011) and, possibly, virus budding as well. Similarly, the ESCRT adaptor protein, Alix, also has been shown to bind K63-linked Ub_2 (Dowlatshahi et al., 2012; Keren-Kaplan et al., 2013). The modification was found to be important for Alix activation, a prerequisite for its ESCRT-III recruitment function and, thereby, for its role in virus budding (Dowlatshahi et al., 2012). These more recent confirmations of K63-linked Ub_2 involvement in events preceding scission machinery recruitment may have been presaged by earlier observations (Strack et al., 2000; Strack et al., 2002; Weiss et al., 2010).

It has been proposed that newly synthesized Gag first accumulates and assembles at the plasma membrane, but a proportion is subsequently internalized via endocytosis (Jouvenet et al., 2008), thus accounting for observations of endosomal localization made by our lab and others (Basyuk et al., 2003; Goff et al., 2003; Nydegger et al., 2003; Sfakianos and Hunter, 2003; Sherer et al., 2003). If so, Ub binding at the N-terminus of the UEV domain might serve to minimize such non-productive endocytosis. If Gag is subject to endocytosis, especially during the early stages of assembly, it might be pertinent that Ku et al.(Ku et al., 2013) identified pauses during formation of HIV-1 VLPs and speculated the existence of a rate-limiting event required for continuation of assembly. Gag itself or key ESCRT-related factors such as Tsg101 or Alix were eliminated as candidates and, instead, temporary shortages of Ub-related enzymatic activity were speculated as possibly responsible, consistent with reports that Ub ligases and DUb activity play a role in HIV-1 budding (Chung et al., 2008; Sette et al., 2010; Sette et al., 2013; Weiss et al., 2010).

In summary, the structure of the Tsg101 and K63-linked Ub_2 complex have provided us with the foundation to differentiate the roles of P(T/S)AP and Ub signaling in Tsg101 function. We showed that Tsg101 P(T/S)AP recognition allows partner recruitment such as Gag or Hrs, while its different modes of Ub_2 interactions can modulate recruitment as well as decide where the complex will be trafficked in the cell. Disruption of Ub_2 recognition by Tsg101 impairs the trafficking of the viral protein Gag, while it has no apparent effect on the cellular protein Hrs. This distinct functional role of Ub signaling provides an excellent target for therapeutics that can block viral production while leaving Tsg101 cellular function intact. Given the broad involvement of Tsg101 and ESCRT machinery in several diverse cellular functions, including virus budding, MVB formation, growth factor signaling down-regulation and cytokinesis, further understanding of the role that Ub and Ub_2 binding play in Tsg101 partner recognition and ESCRT cargo sorting could provide critical new insights necessary for selective targeting of its participation in infectious diseases and cancer.

STAR METHODS

RESOURCE AVAILABILITY

Lead contact—Further information and requests for resources and reagents should be resource requests should be directed to and will be fulfilled by the lead contact, Dr. Nico Tjandra (tjandran@nhlbi.nih.gov).

Materials Availability—Any unique reagents, plasmids or materials generated in this study are available upon reasonable request submitted to the lead contact.

Data and code availability—Structure coordinates have been deposited in the Protein Data Bank (PDB) with accession code 6UD0 and are publicly available as of the date of this publication. NMR chemical shifts and structural restraints have been deposited in the Biological Magnetic Resonance Data Bank (BMRB) with accession code 30675 and are publicly available.

This paper does not report original code.

Any additional information required to reanalyze the data reported in this paper is available from the lead contact upon request

EXPERIMENTAL MODEL AND SUBJECT DETAILS

Cell Lines—HeLa (ATCC CCL-2) cells were grown in Dulbecco's modified Eagle medium supplemented with fetal bovine serum (10%) and antibiotics (1%) to 70% confluency at 37 °C prior to drug treatment or transfection.

Rosetta™(DE3)pLysS (DE3) Competent Cells were were grown overnight at 37°C in 1 L of Luria-Bertani broth (MP Biomedicals) containing 100 μg/mL ampicillin (Sigma) and 34 μg/mL chloramphenicol (Sigma). After dilution with 1 L of media containing the antibiotics, the cells were grown at 37°C for an additional hour before induction with 1 mM IPTG (Calbiochem) for 3 hr at 37°C.

Saccharomyces cerevisiae strain Y190 colonies transformed with plasmids of interest were inoculated into liquid yeast minimal media lacking leucine and tryptophan to maintain selective pressure, grown overnight, and then supplemented with yeast extract peptone dextrose media to promote rapid growth for 4 hr at 30 C.

METHOD DETAILS

Production of Tsg101 and ubiquitin monomers—Wild-type Tsg101 ubiquitin E2 variant (UEV) domain (residues 2–145) and wild-type ubiquitin were expressed in Rosetta 2 (DE3) pLysS *Escherichia coli* competent cells (EMD Millipore) grown in either Luria-Bertani broth (MP Biomedicals) or M9 media containing 50 mg L^{-1} kanamycin (Sigma) and 34 mg L^{-1} chloramphenicol (Sigma). Cells grown in M9 media were supplemented with $^{15}NH_4Cl$ and natural abundance glucose. As described previously (Strickland et al., 2017), Tsg101 protein was purified as a His-tagged construct using nickel affinity chromatography followed by a tobacco etch virus (TEV) protease cleavage step and a second pass through

nickel affinity chromatography to remove the His_6 tag. Labeled and unlabeled proteins were then passed over a size-exclusion column as a final purification step. The T14C mutant ubiquitin plasmid was produced using a Quik-Change site-directed mutagenesis kit (Stratagene), and was expressed and purified either as natural abundance or as a ^{15}N-labeled protein, as described previously for a different ubiquitin cysteine mutant (Opina et al., 2016). Monomeric human ubiquitin mutants (used to form diubiquitin chains), containing K48R, K63R, D77, K63R/T14C, or T14C/D77 mutations were expressed in Rosetta 2 (DE3) pLysS *Escherichia coli* cells, either as natural abundance or as a ^{15}N-labeled protein (Varadan et al., 2002) using growth conditions as described above and purified as previously described (Pickart and Raasi, 2005). Briefly, after emulsification, cell debris was removed by ultracentrifugation (125,000 × g for 60 min) at 4°C. The supernatant was heated to 60–65°C for 5 min while stirring, clarified by centrifugation at 125,000 × g for 60 min at 4°C, and its pH was adjusted to 8.6. Poly ubiquitints were further purified by ion exchange and size exclusion chromatography before experimental use.

Production of K48- and K63-linked chains—The following ubiquitin chains were produced and purified: unlabeled K48-linked Ub_2, unlabeled K63-linked Ub_2, and unlabeled K63-linked Ub_3 (for chemical shift perturbations of Tsg101), unlabeled K63-linked Ub_2 containing T14C mutation in either the proximal or the distal Ub unit (for Tsg101 pseudocontact shifts), K63-linked Ub_2 with proximal Ub unit ^{15}N-enriched, K63-linked Ub_2 with distal Ub unit ^{15}N-enriched (for chemical shift perturbations of Ub_2). The dimers were assembled from respective recombinant Ub monomers through controlled polyubiquitin chain synthesis using enzyme-catalyzed Ub-conjugation reactions as detailed elsewhere (Pickart and Raasi, 2005; Varadan et al., 2005; Varadan et al., 2004; Varadan et al., 2002). Briefly, these reactions used human Ub-activating E1 enzyme (Uba1) in combination with respective linkage-selective Ub-conjugating E2 enzymes: human Ube2K (aka E2-25K) for K48-linked chains and yeast Ubc13/Mms2 complex for K63-linked chains. To control the chain length/assembly, the synthesis employed Ub variants containing chain-terminating point mutations: UbD77 as the proximal Ub and UbK48R or UbK63R as the distal Ub (for K48- or K63-linkage, respectively), thus resulting in Ub dimers with desired linkages. Ub unit-selective ^{15}N-labeling was achieved by using ^{15}N-enriched Ub as the proximal or distal Ub and unlabeled Ub as the distal or proximal Ub, respectively. A similar assembly scheme was used to produce Ub dimers containing T14C mutation on the proximal or distal Ub unit. The dimer products were separated from unreacted monomers by cation exchange chromatography and verified by ESI-MS and SDS PAGE.

K63-linked Ub_3 was assembled from wild-type Ub in a conjugation reaction catalyzed by E1 and Ubc13/Mms2. The reaction was quenched after ~4 hours by adding 10 molar excess of DTT followed by a few drops of glacial acetic acid and subsequent centrifugation for 10 minutes. The trimer was separated from other chains and unreacted monomer by size exclusion chromatography and confirmed by ESI-MS and SDS-PAGE. Unfortunately we found that K63-linked Ub_3 show significant aggregation at concentration above 7μM. The aggregation bands could be observed even in the SDS-PAGE. Therefore the K63-linked Ub_3 was not used in our NMR study.

Production of linear diubiquitin protein—A linear diubiquitin (N-Ub_2) expression vector was engineered using the In-Fusion® (Clontech) recombinational cloning approach. A second ubiquitin coding sequence was seamlessly inserted in-frame downstream to a ubiquitin cDNA already present in the pET-21a destination vector. The primers, used to produce the PCR products for both the insert and the destination vector, were designed using the SnapGene® In-Fusion cloning tool (GSL Biotech) and synthesised by Eurofins. The ligation independent cloning was carried out following Clontech's recommendation. The integrity of the Ub_2 coding sequence was verified (Macrogen, USA). Rosetta™(DE3)pLysS competent cells (Novagen), transformed with the Ub_2 coding plasmid, were grown overnight at 37°C in 1 L of Luria-Bertani broth (MP Biomedicals) containing 100 μg/mL ampicillin (Sigma) and 34 μg/mL chloramphenicol (Sigma). After dilution with 1 L of media containing the antibiotics, the cells were grown at 37°C for an additional hour before induction with 1 mM IPTG (Calbiochem) for 3 hr at 37°C. The cell pellet, harvested at 6,000 rpm for 20 min at 15°C, was resuspended in 100 mM Tris·HCl (pH 7.4), 10% (v/v) glycerol and one tablet of EDTA-free complete protease inhibitor (Roche Diagnostics) and disrupted by two passages through an M-110P homogenizer (Microfluidics™). Cell debris removal was carried out at 125,000 × g for 60 min at 4°C. The supernatant was heated to 60–65°C for 5 min while stirring, clarified by centrifugation at 125,000 × g for 60 min at 4°C, and its pH was adjusted to 8.6 by addition of Tris base. Ub_2-was further purified by ion exchange chromatography on an Akta FPLC (GE Healthcare). The supernatant was filtered through a 5 mL HiTrap™ Q HP column (GE Healthcare) equilibrated with 50 mM Tris·HCl (pH 8.6) and 50 mM NaCl. The Ub_2-containing flow-though was adjusted to pH 4.5 with acetic acid and loaded onto a 5 mL HiTrap™ SP HP column (GE Healthcare) equilibrated with 50 mM sodium acetate (pH 4.5). Ub_2-was eluted, using a 100 mL linear gradient to 500 mM NaCl, as a single peak at a maximum NaCl concentration of ~300 mM. The protein-containing fractions considered pure by SDS-PAGE were pooled, concentrated, and exchanged into 4 M urea (Amicon, 3,000 MWCO; Millipore). Final polishing was performed by size exclusion chromatography using a HiLoad 26/60 Superdex 75 prep grade column (GE Healthcare) and isocratic elution in PBS. The protein-containing fractions were pooled after SDS-PAGE analysis and the identity of the protein was confirmed by MS analysis (Agilent 6224 ESI-TOF LC-MS). Linear Ub_2 was dialyzed exhaustively against water, lyophilized, and stored at −20°C.

Samples for NMR binding studies—^{1}H-^{15}N-heteronuclear single quantum coherence spectroscopy (HSQC) experiments were used to measure ^{15}N-Tsg101 UEV chemical shift perturbations, upon addition of natural abundance K63-Ub_2, K48-Ub_2, or linear Ub_2. K63-Ub_2 ubiquitin chemical shift perturbations were measured using ^{15}N-labeling on either the distal or proximal Ub of Ub_2, upon addition of natural abundance Tsg101 UEV. All proteins were present at a 200 μM concentration in a 1:1 ratio in buffer containing 20 mM potassium phosphate (pH 5.8), 50 mM NaCl, and 7% $^{2}H_2O$. Results for Ub_1 were adapted from Strickland et al., 2017 and shown again here, in Fig. 2, for direct comparison (all experimental conditions were identical) (Strickland et al., 2017).

Samples for NMR pseudocontact shift studies—Natural abundance T14C mutated Ub_1 or K63-Ub_2 (mutated on either the distal or proximal Ub) were tagged with diamagnetic

Lu-DOTA-M8-SPy or paramagnetic Tm-DOTA-M8-SPy, as described previously for a different ubiquitin mutant ($^{S57C}Ub_1$) (Opina et al., 2016). Briefly, the tag was attached covalently using disulfide bond exchange at room temperature for 16 hours, before purification. Tagged Ub_2 samples were added to ^{15}N-Tsg101 at a 1:1 ratio (final Tsg101 concentration of 125 μM), concentrated in an Amicon ultracentrifugal filter (MWCO 3 kDa) to 250 μL for NMR measurement in a Shigemi tube. Tagged Ub_1 was added to ^{15}N-Tsg101 at a 1:2 ratio (final Tsg101 concentration of 88 μM). All samples were in a buffer containing 20 mM potassium phosphate (pH 5.8), 50 mM NaCl, 7% ^2H_2O.

Samples for CPMG experiments—^{15}N R_2 CPMG experiments were measured using 300 μM ^{15}N-Tsg101 UEV, either in the free form or in complex with the 'PTAP' peptide in a 1:1 ratio. The 'PTAP' peptide was present at natural abundance, purchased from bioSYNTHESIS with the sequence Ace-NFLQSRPEPTAPPEE-$CONH_2$. The stock solution of the peptide was made by dissolving the peptide powder in a buffer containing 20 mM potassium phosphate (pH 5.8), 50 mM NaCl, and 7% ^2H_2O. The concentration of the stock solution was determined by 1D proton NMR comparison with a sister peptide (Ace-NFLQSRPEPTAPPEESW-$CONH_2$, bioSYNTHESIS) containing an added tryptophan, whose concentration was previously determined using A_{280nm}.

NMR spectroscopy—^{1}H-^{15}N-HSQC spectra were acquired for chemical shift perturbation experiments at 300 K on Bruker 600 and 800 MHz spectrometers equipped with cryoprobes. Chemical shift titrations at 300K were monitored following each serial addition of monoubiquitin using ^{1}H-^{15}N-HSQC spectra acquired on a Bruker 900 MHz spectrometer. HSQC spectra for pseudocontact shift experiments were measured at 600 MHz, while CPMG experiments were measured at 800 MHz. Spectra were processed using NMRPipe (Delaglio et al., 1995) and analyzed using CCPN Analysis 2.4.1 (Vranken et al., 2005). NMR resonances of Tsg101 UEV domain and K63-Ub_2 Ubs were assigned as described previously (Strickland et al., 2017). Protein complex assignments were completed using titrations (0.25x, 0.50x, 0.75x, and 1x). The PTAP/Tsg101 complex chemical shifts for CPMG experiments were compared to a previous titration to confirm a 1:1 ratio and to assign the peaks (Strickland et al., 2017).

Plasmids and antibodies—pCMV-Gag-EGFP encoding HIV-1 Gag C-terminally tagged with green fluorescent protein (GFP) and pLLEXP1-hTsg101-Myc encoding full-length human Tsg101 C-terminally tagged with Myc were previously described.(Goff et al., 2003) Yeast plasmids pGADTsg101 and pGBT HIV-1 Gag were constructed by subcloning from pLLEXP1-hTsg101-Myc and pCMV-Gag-EGFP, respectively. Mutations were created in the Tsg101 constructs using site directed mutagenesis and confirmed by DNA sequencing. Antibodies used for microscopy were anti-Myc (Santa Cruz Biotechnology, 9E10) and secondary antibody goat anti-mouse IgG tagged with Texas Red (Molecular Probes).

Fluorescence Microscopy—Cells were prepared and analyzed as previously described (Strickland et al., 2017). HeLa cells were transfected (Sigma, X-treme GENE) with pCMV-Gag-EGFP with pLLEXP1-hTsg101-Myc. Cells were fixed in 4% formaldehyde (Sigma) and permeabilized in 0.1% Triton X-100. Tsg101 was detected in the samples by

indirect immunofluorescence using anti-Myc Mab (Santa Cruz Biotechnology, 9E10) and Texas Red anti-mouse IgG (Molecular Probes). Nuclei were stained with DAPI (Thermo Scientific). Cells were fixed with anti-fade mountant (Molecular Probes). Images were captured on an inverted fluorescence/differential-interference contrast (dic) Zeiss Axiovert 200M deconvolving fluorescence microscope operated by Zeiss AxioVision Version 4.5 software and deconvolved by using the constrained iterative method. Protein co-localization was assessed in the entire co-transfected cell with Pearson's coefficient of correlation using NIH Image J, JACoP plugin software (Bolte and Cordelieres, 2006). Pearson's values were analyzed using Prism7's t-test statistical software (GraphPad.com).

Yeast 2-Hybrid system—HIV-1 Gag wild-type and Tsg101 wild-type and mutants were tested for protein-protein interactions using the Matchmaker GAL4 Yeast Two Hybrid β-galactosidase assay (Clontech Laboratories, Inc.) using *Saccharomyces cerevisiae* strain Y190. pGAD and pGBT plasmids containing Tsg101 or Gag sequences, respectively, were co-transformed into Y190 and selected on yeast minimal media plates lacking leucine and tryptophan. Colonies were inoculated into liquid yeast minimal media lacking leucine and tryptophan to maintain selective pressure, grown overnight, and then supplemented with yeast extract peptone dextrose media to promote rapid growth for 4 hr at 30 C. Cell density was measured by reading OD_{650nm}. Cells (1 ml) were washed in Z Buffer (60 mM Na_2HPO_4, 40 mM NaH_2PO_4, 10 mM KCl, 1 mM $MgSO_4$) and resuspended in 0.5 ml reaction mix (Z buffer, 38 mM β-mercaptoethanol, 0.02% SDS, 0.02% Triton X-100, 1mg/ml ortho-nitrophenyl β—galactoside) for 18 hr. Reactions (0.5 ml) were stopped by the addition of 0.25 ml of 1 M Na_2CO_3, cells pelleted, and the β—Gal signal read at OD_{415nm}. For each assay, a blank consisting of reaction mix alone was run in parallel and subtracted from the samples. For the analysis of the Tsg101 mutants, two to three separate plasmid constructs were transformed and one or two transformants for each tested, resulting in six to sixteen measurements in two to five separate assays per mutant. Values were adjusted for OD_{650nm} and normalized to co-transformants of Tsg101 WT and Gag WT run in parallel. Co-transformants of Tsg101 WT and Gag P7L as well as Tsg101 WT and Gag 2XPTAP were also run in parallel as controls for each assay.

QUANTIFICATION AND STATISTICAL ANALYSIS

CPMG experiments—The R_2 CPMG experiments (Loria et al., 1999) were measured with τ_{cp} of 0.315 ms and 1.875 ms for the free form of Tsg101, and 0.3125 ms and 1.875 ms for Tsg101 in complex with the PTAP peptide. τ_{cp} is defined as one-half of the duration time between two successive 180° ^{15}N pulses during spin echo delays (Ishima and Torchia, 1999). For each τ_{cp} value, a relaxation rate was derived using peak heights from two time points points (t_1 = 4 ms and t_2 = 60 ms for Tsg101 in complex with the PTAP peptide, and t_1 = 4 ms and t_2 = 30 ms for the free form of Tsg101), according to the following equation:

$$R_2^{CPMG} = -\left(\frac{1}{t_2 - t1}\right)\ln\left(\frac{I_{t2}}{I_{t1}}\right)$$

where I_{t1} and I_{t2} are the peak heights derived from the experiments measured at each time point, t_1 and t_2, respectively. CPMG ratios were then calculated from R_2 values measured at

two τ_{cp} values. CPMG error bars were derived from RMSD values for noise-free regions of the spectra obtained using NMRFAM-Sparky v. 1.414 (Lee et al., 2015) (powered by Sparky 3.135)(Goddard).

Errors were propagated using the following equation:

$$Error^{R_2^{CPMG}} = R_2^{CPMG}\sqrt{\left(\frac{RMSD_{t1}}{I_{t1}}\right)^2 + \left(\frac{RMSD_{t2}}{I_{t2}}\right)^2}$$

Chemical shift perturbation restraints—Chemical shift perturbations (CSPs) were calculated using the equation and method described in Strickland et al., 2017. In short, the CSPs were calculated according to the following equation: $\sqrt{[(H_{complex} - H_{free})^2 + (\alpha(N_{complex} - N_{free}))^2]}$, where α is a scaling factor equal to 0.13, calculated from $\alpha = (H_{max} - H_{min}) / (N_{max} - N_{min})$, where $H_{complex}$ and $N_{complex}$ describe the H and N chemical shifts in the complexed form, H_{free} and N_{free} describe the H and N chemical shifts in the free form, H_{max} and N_{max} describe the largest chemical shifts from the ^{1}H-^{15}N-HSQC spectrum of Tsg101 in the free form, and H_{min} and N_{min} describe the smallest chemical shifts.The cutoff for large chemical shift perturbations was 1.5 standard deviations from zero. Prolines and residues with broadened NMR resonances are not included in the analysis. Chemical shift perturbations were used for determining the complex of Tsg101 and K63-Ub_2. All significant CSPs for Tsg101 and K63-Ub_2 were used as an ambiguous distance restraints as described previously (Clore and Schwieters, 2003; Strickland et al., 2016b). Briefly, any residue that registered a significant CSP would be restrained to within 1.8–5 Å from the binding interface of its binding partner using an NOE distance restraint.

Pseudocontact shift restraints—Tsg101 pseudocontact shifts were calculated as the difference in proton chemical shifts for Tsg101 measured in the presence of diamagnetic or paramagnetic lanthanide-tagged Ub_1 or K63-Ub_2, as described previously for the NPr:Enzyme I^{Ntr} complex (Strickland et al., 2016b). Diubiquitin samples were labeled with Lu- or Tm-M8-DOTA-SPy, tagged either on the distal or proximal Ub of diubiquitin at residue T14C. Each experiment was measured twice to obtain an average chemical shift and standard deviation. Errors were derived according to the following equation: Error = ($S.D._{dia}$ + $S.D._{para}$).

K63-Ub_2 and Tsg101 setup for calculation—K63-Ub_2 and Tsg101 structures used in the calculation were derived from PDB structures 3H7P/2MJB and 1S1Q, respectively (Maltsev et al., 2014; Sundquist et al., 2004; Weeks et al., 2009). Tsg101 was represented by the crystal structure of Tsg101 in complex with monoubiquitin (1S1Q), with the monoubiquitin molecule removed. The 2MJB solution-state NMR structure of monoubiquitin is considered to be the highest quality ubiquitin structure available (Maltsev et al., 2014) and so was used to define the diubiquitin coordinates. The monoubiquitin was duplicated and overlaid on the 3H7P crystal structure of K63-Ub_2 using the refRMSD term of Xplor-NIH (Schwieters et al., 2006; Schwieters et al., 2003). The linker was defined using a diubiquitin linker patch in Xplor-NIH. The K63-Ub_2 structure was modified in Xplor-NIH by addition of Ln-M8-DOTA-SPy tags (TSAP isomer) at position T14C of both

the distal and proximal Ubs as described previously (Strickland et al., 2016a), and by K63R mutation of the distal Ub and +D77 of the proximal Ub to match the sample used for PCS measurement. Protons were added to the Tsg101 crystal structure using Xplor-NIH.

Tsg101:K63-Ub$_2$ initial structure calculation—The Tsg101 and K63-Ub$_2$ structures were calculated using the simulated annealing protocol of Xplor-NIH 2.48. Tsg101 PCS restraints were used for both the distal- and proximal-tagged Ub of K63-Ub$_2$ simultaneously. PCS magnetic susceptibility tensors were calculated using the varTensor module then held fixed throughout. CSPs were used as ambiguous distance restraints using the NOE potential. Other potentials included volume of gyration, contact, hydrogen bonding, Van der Waals, bond, angle, and improper terms. Dynamics were performed in torsion angle space, with Tsg101 and residues 1–72 of the distal Ub of K63-Ub$_2$ held fixed. The starting positions of Tsg101 and the distal Ub were determined by alignment to the structure of Ub$_1$ in complex with Tsg101 (PDB: 1S1Q) (Sundquist et al., 2004). Residues 1–72 of the proximal Ub of K63-Ub$_2$ were grouped and allowed to move as a rigid body. Residues 73–76 or 73–77 of the K63-Ub$_2$ distal and proximal Ubs, respectively, were allowed to move freely. Final minimization in cartesian space was carried out with mobile side-chains (excepting tagged residues T14C on both K63-Ub$_2$ Ubs). Five docking attempts were made for each structure before refinement. 100 structures were calculated in total, with the ten lowest in overall energy used for further analysis.

Tsg101:K63-Ub$_2$ ensemble refinement—The ten lowest energy structures from the initial calculation of the Tsg101: K63-Ub$_2$ complex were found to be clustered into two major categories, each with the proximal Ub K63-Ub$_2$ bound to a different region of Tsg101. The lowest overall energy structures from each cluster were used as input for an Xplor-NIH ensemble refinement with two ensemble members, weighted equally (0.5). A 3 Å refRMSD term was used to restrain the distal Ub of K63-Ub$_2$ (residues 1–72) and Tsg101 to their initial position. The PCS susceptibility tensor parameters were initially fixed (distal Ub $\chi_a = 8.07 \times 10^{-33}$ m^3, $\chi_r = 1.37 \times 10^{-33}$ m^3, proximal Ub $\chi_a = 1.94 \times 10^{-32}$ m^3, $\chi_r = 1.14 \times 10^{-32}$ m^3) and then varied during final minimization. The final magnetic susceptibility tensor values were for distal Ub $\chi_a = 7.89 \times 10^{-33}$ m^3, $\chi_r = 1.60 \times 10^{-33}$ m^3, for proximal Ub $\chi_a = 1.88 \times 10^{-32}$ m^3, $\chi_r = 1.25 \times 10^{-32}$ m^3. PCS were calculated as an ensemble. CSPs for Tsg101 residues were split into three categories – distal, proximal cluster 1, and proximal cluster 2. Distal CSPs were calculated as an ensemble, whereas CSPs for proximal clusters 1 and 2 were weighted to correspond to the appropriate ensemble member. All other energy terms were calculated as an ensemble. Fixing and grouping of the Ub units during the dynamics stage were as for the initial calculation protocol for the complex. During final minimization, residues 1–72 of both K63-Ub$_2$ Ub units and all of Tsg101 were fixed, while side-chains could move (excepting residue T14C of the distal Ub). The ‘repel’ energy term was used during refinement to avoid atomic clashes. 100 structure ensemble pairs were calculated in total, with the ten lowest in energy used for structure validation. Xplor-NIH was used to removed the tag from the distal and proximal Ubs of Ub$_2$ by mutation (C14T) and energy minimization of residue T14 prior to validation and submission to the Protein Data Bank. Validation was carried out using the Protein Structure Validation Suite web server (Bhattacharya et al., 2007) (Table 1).

Supplementary Material

Refer to Web version on PubMed Central for supplementary material.

ACKNOWLEDGEMENTS

We thank Dr. Duck-Yeon Lee of the Biochemistry Core Facility and Yi He of the Laboratory of Structural Biophysics at the NHLBI for expertise and advice regarding LC-MS and for the growth of *E. coli* for production of isotopically-labeled Tsg101, respectively. We thank Rohith Rajasekaran of the Biochemistry and Biophysics Center (NHLBI) for producing linear diubiquitin. We thank Dr. Charles D. Schwieters and Dr. Guillermo A. Bermejo of the Center for Information Technology at the NIH for expertise regarding NMR structure calculations with Xplor-NIH. We also thank Drs. Lorna Ehrlich (SBU) and James Konopka (SBU) for helpful discussions. These investigations were supported by funds from the National Institutes of Health (NIH) National Institute Allergy and Infectious Diseases R01 AI150489 to CAC and R01 GM065334 to DF; Intramural Research Programs of the National Heart, Lung, and Blood Institute (NHLBI) of the NIH to NT. The manuscript content is solely the responsibility of the authors.

REFERENCES

Adell MA, Vogel GF, Pakdel M, Muller M, Lindner H, Hess MW, and Teis D (2014). Coordinated binding of Vps4 to ESCRT-III drives membrane neck constriction during MVB vesicle formation. J Cell Biol 205, 33–49. [PubMed: 24711499]

Ahmed I, Akram Z, Iqbal HMN, and Munn AL (2019). The regulation of Endosomal Sorting Complex Required for Transport and accessory proteins in multivesicular body sorting and enveloped viral budding - An overview. Int J Biol Macromol 127, 1–11. [PubMed: 30615963]

Alam SL, Sun J, Payne M, Welch BD, Blake BK, Davis DR, Meyer HH, Emr SD, and Sundquist WI (2004). Ubiquitin interactions of NZF zinc fingers. The EMBO journal 23, 1411–1421. [PubMed: 15029239]

Baldys A, and Raymond JR (2009). Critical role of ESCRT machinery in EGFR recycling. Biochemistry 48, 9321–9323. [PubMed: 19673488]

Basyuk E, Galli T, Mougel M, Blanchard JM, Sitbon M, and Bertrand E (2003). Retroviral genomic RNAs are transported to the plasma membrane by endosomal vesicles. Dev Cell 5, 161–174. [PubMed: 12852860]

Bhattacharya A, Tejero R, and Montelione GT (2007). Evaluating protein structures determined by structural genomics consortia. Proteins 66, 778–795. [PubMed: 17186527]

Bilodeau PS, Urbanowski JL, Winistorfer SC, and Piper RC (2002). The Vps27p Hse1p complex binds ubiquitin and mediates endosomal protein sorting. Nat Cell Biol 4, 534–539. [PubMed: 12055639]

Bolte S, and Cordelieres FP (2006). A guided tour into subcellular colocalization analysis in light microscopy. J Microsc 224, 213–232. [PubMed: 17210054]

Carter CA (2002). Tsg101: HIV-1's ticket to ride. Trends Microbiol 10, 203–205. [PubMed: 11973141]

Chen VB, Arendall WB 3rd, Headd JJ, Keedy DA, Immormino RM, Kapral GJ, Murray LW, Richardson JS, and Richardson DC (2010). MolProbity: all-atom structure validation for macromolecular crystallography. Acta Crystallogr D Biol Crystallogr 66, 12–21. [PubMed: 20057044]

Chung HY, Morita E, von Schwedler U, Muller B, Krausslich HG, and Sundquist WI (2008). NEDD4L overexpression rescues the release and infectivity of human immunodeficiency virus type 1 constructs lacking PTAP and YPXL late domains. Journal of virology 82, 4884–4897. [PubMed: 18321968]

Clague MJ, and Urbe S (2010). Ubiquitin: same molecule, different degradation pathways. Cell 143, 682–685. [PubMed: 21111229]

Clore GM, and Schwieters CD (2003). Docking of protein-protein complexes on the basis of highly ambiguous intermolecular distance restraints derived from 1H/15N chemical shift mapping and backbone 15N-1H residual dipolar couplings using conjoined rigid body/torsion angle dynamics. J Am Chem Soc 125, 2902–2912. [PubMed: 12617657]

Cornilescu G, Marquardt JL, Ottiger M, and Bax A (1998). Validation of protein structure from anisotropic carbonyl chemical shifts in a dilute liquid crystalline phase. J Am Chem Soc 120, 6836–6837.

Critchley WR, Pellet-Many C, Ringham-Terry B, Harrison MA, Zachary IC, and Ponnambalam S (2018). Receptor Tyrosine Kinase Ubiquitination and De-Ubiquitination in Signal Transduction and Receptor Trafficking. Cells 7.

Delaglio F, Grzesiek S, Vuister GW, Zhu G, Pfeifer J, and Bax A (1995). Nmrpipe - a Multidimensional Spectral Processing System Based on Unix Pipes. Journal of biomolecular NMR 6, 277–293. [PubMed: 8520220]

Dowlatshahi DP, Sandrin V, Vivona S, Shaler TA, Kaiser SE, Melandri F, Sundquist WI, and Kopito RR (2012). ALIX is a Lys63-specific polyubiquitin binding protein that functions in retrovirus budding. Dev Cell 23, 1247–1254. [PubMed: 23201121]

Eyster CA, Cole NB, Petersen S, Viswanathan K, Fruh K, and Donaldson JG (2011). MARCH ubiquitin ligases alter the itinerary of clathrin-independent cargo from recycling to degradation. Mol Biol Cell 22, 3218–3230. [PubMed: 21757542]

Frankel EB, and Audhya A (2018). ESCRT-dependent cargo sorting at multivesicular endosomes. Semin Cell Dev Biol 74, 4–10. [PubMed: 28797838]

Garrus JE, von Schwedler UK, Pornillos OW, Morham SG, Zavitz KH, Wang HE, Wettstein DA, Stray KM, Cote M, Rich RL, et al. (2001). Tsg101 and the vacuolar protein sorting pathway are essential for HIV-1 budding. Cell 107, 55–65. [PubMed: 11595185]

Goddard TD K. DG SPARKY 3. University of California, San Francisco.

Goff A, Ehrlich LS, Cohen SN, and Carter CA (2003). Tsg101 control of human immunodeficiency virus type 1 Gag trafficking and release. Journal of virology 77, 9173–9182. [PubMed: 12915533]

Gottlinger HG, Dorfman T, Sodroski JG, and Haseltine WA (1991). Effect of mutations affecting the p6 gag protein on human immunodeficiency virus particle release. Proceedings of the National Academy of Sciences of the United States of America 88, 3195–3199. [PubMed: 2014240]

Gruenberg J, and Stenmark H (2004). The biogenesis of multivesicular endosomes. Nat Rev Mol Cell Biol 5, 317–323. [PubMed: 15071556]

Hanson PI, and Cashikar A (2012). Multivesicular body morphogenesis. Annu Rev Cell Dev Biol 28, 337–362. [PubMed: 22831642]

Hurley JH (2008). ESCRT complexes and the biogenesis of multivesicular bodies. Curr Opin Cell Biol 20, 4–11. [PubMed: 18222686]

Im YJ, Kuo L, Ren X, Burgos PV, Zhao XZ, Liu F, Burke TR Jr., Bonifacino JS, Freed EO, and Hurley JH (2010). Crystallographic and functional analysis of the ESCRT-I /HIV-1 Gag PTAP interaction. Structure 18, 1536–1547. [PubMed: 21070952]

Ishima R, and Torchia DA (1999). Estimating the time scale of chemical exchange of proteins from measurements of transverse relaxation rates in solution. Journal of biomolecular NMR 14, 369–372. [PubMed: 10526408]

Jouvenet N, Bieniasz PD, and Simon SM (2008). Imaging the biogenesis of individual HIV-1 virions in live cells. Nature 454, 236–240. [PubMed: 18500329]

Katzmann DJ, Babst M, and Emr SD (2001). Ubiquitin-dependent sorting into the multivesicular body pathway requires the function of a conserved endosomal protein sorting complex, ESCRT-I. Cell 106, 145–155. [PubMed: 11511343]

Keizers PH, Mersinli B, Reinle W, Donauer J, Hiruma Y, Hannemann F, Overhand M, Bernhardt R, and Ubbink M (2010). A solution model of the complex formed by adrenodoxin and adrenodoxin reductase determined by paramagnetic NMR spectroscopy. Biochemistry 49, 6846–6855. [PubMed: 20695524]

Keren-Kaplan T, Attali I, Estrin M, Kuo LS, Farkash E, Jerabek-Willemsen M, Blutraich N, Artzi S, Peri A, Freed EO, et al. (2013). Structure-based in silico identification of ubiquitin-binding domains provides insights into the ALIX-V:ubiquitin complex and retrovirus budding. The EMBO journal 32, 538–551. [PubMed: 23361315]

Kim HJ, Taylor LJ, and Bar-Sagi D (2007). Spatial regulation of EGFR signaling by Sprouty2. Curr Biol 17, 455–461. [PubMed: 17320394]

Kim MS, Kim JA, Song HK, and Jeon H (2006). STAM-AMSH interaction facilitates the deubiquitination activity in the C-terminal AMSH. Biochem Biophys Res Commun 351, 612–618. [PubMed: 17078930]

Koonin EV, and Abagyan RA (1997). TSG101 may be the prototype of a class of dominant negative ubiquitin regulators. Nat Genet 16, 330–331. [PubMed: 9241264]

Ku PI, Miller AK, Ballew J, Sandrin V, Adler FR, and Saffarian S (2013). Identification of pauses during formation of HIV-1 virus like particles. Biophys J 105, 2262–2272. [PubMed: 24268138]

Lee W, Tonelli M, and Markley JL (2015). NMRFAM-SPARKY: enhanced software for biomolecular NMR spectroscopy. Bioinformatics 31, 1325–1327. [PubMed: 25505092]

Leonard D, Hayakawa A, Lawe D, Lambright D, Bellve KD, Standley C, Lifshitz LM, Fogarty KE, and Corvera S (2008). Sorting of EGF and transferrin at the plasma membrane and by cargo-specific signaling to EEA1-enriched endosomes. Journal of cell science 121, 3445–3458. [PubMed: 18827013]

Loria JP, Rance M, and Palmer AG (1999). A relaxation-compensated Carr-Purcell-Meiboom-Gill sequence for characterizing chemical exchange by NMR spectroscopy. J Am Chem Soc 121, 2331–2332.

Lu Q, Hope LW, Brasch M, Reinhard C, and Cohen SN (2003). TSG101 interaction with HRS mediates endosomal trafficking and receptor down-regulation. Proc Natl Acad Sci U S A 100, 7626–7631. [PubMed: 12802020]

Maltsev AS, Grishaev A, Roche J, Zasloff M, and Bax A (2014). Improved cross validation of a static ubiquitin structure derived from high precision residual dipolar couplings measured in a drug-based liquid crystalline phase. J Am Chem Soc 136, 3752–3755. [PubMed: 24568736]

Martin-Serrano J, Zang T, and Bieniasz PD (2001). HIV-1 and Ebola virus encode small peptide motifs that recruit Tsg101 to sites of particle assembly to facilitate egress. Nat Med 7, 1313–1319. [PubMed: 11726971]

McCullough J, Row PE, Lorenzo O, Doherty M, Beynon R, Clague MJ, and Urbe S (2006). Activation of the endosome-associated ubiquitin isopeptidase AMSH by STAM, a component of the multivesicular body-sorting machinery. Curr Biol 16, 160–165. [PubMed: 16431367]

Medina G, Zhang Y, Tang Y, Gottwein E, Vana ML, Bouamr F, Leis J, and Carter CA (2005). The functionally exchangeable L domains in RSV and HIV-1 Gag direct particle release through pathways linked by Tsg101. Traffic 6, 880–894. [PubMed: 16138902]

Mishra P, Barnes CA, Strickland M, and Tjandra N (2018). Solvent saturation transfer to proteins (SSTP) for structural and functional characterization of proteins. J Biomol NMR 70, 11–20. [PubMed: 29189927]

Nydegger S, Foti M, Derdowski A, Spearman P, and Thali M (2003). HIV-1 egress is gated through late endosomal membranes. Traffic 4, 902–910. [PubMed: 14617353]

Opina AC, Strickland M, Lee YS, Tjandra N, Andrew Byrd R, Swenson RE, and Vasalatiy O (2016). Analysis of the isomer ratios of polymethylated-DOTA complexes and the implications on protein structural studies. Dalton Trans 45, 4673–4687. [PubMed: 26857249]

Pickart CM, and Raasi S (2005). Controlled synthesis of polyubiquitin chains. Methods Enzymol 399, 21–36. [PubMed: 16338346]

Piper RC, and Luzio JP (2007). Ubiquitin-dependent sorting of integral membrane proteins for degradation in lysosomes. Curr Opin Cell Biol 19, 459–465. [PubMed: 17689064]

Ponting CP, Cai YD, and Bork P (1997). The breast cancer gene product TSG101: a regulator of ubiquitination? J Mol Med (Berl) 75, 467–469. [PubMed: 9253709]

Pornillos O, Alam SL, Rich RL, Myszka DG, Davis DR, and Sundquist WI (2002). Structure and functional interactions of the Tsg101 UEV domain. EMBO J 21, 2397–2406. [PubMed: 12006492]

Pornillos O, Higginson DS, Stray KM, Fisher RD, Garrus JE, Payne M, He GP, Wang HE, Morham SG, and Sundquist WI (2003). HIV Gag mimics the Tsg101-recruiting activity of the human Hrs protein. The Journal of cell biology 162, 425–434. [PubMed: 12900394]

Schwieters CD, Kuszewski JJ, and Clore GM (2006). Using Xplor-NIH for NMR molecular structure determination. Prog Nucl Mag Res Sp 48, 47–62.

Schwieters CD, Kuszewski JJ, Tjandra N, and Clore GM (2003). The Xplor-NIH NMR molecular structure determination package. Journal of magnetic resonance 160, 65–73. [PubMed: 12565051]

Sette P, Jadwin JA, Dussupt V, Bello NF, and Bouamr F (2010). The ESCRT-associated protein Alix recruits the ubiquitin ligase Nedd4-1 to facilitate HIV-1 release through the LYPXnL L domain motif. Journal of virology 84, 8181–8192. [PubMed: 20519395]

Sette P, Nagashima K, Piper RC, and Bouamr F (2013). Ubiquitin conjugation to Gag is essential for ESCRT-mediated HIV-1 budding. Retrovirology 10, 79. [PubMed: 23895345]

Sfakianos JN, and Hunter E (2003). M-PMV capsid transport is mediated by Env/Gag interactions at the pericentriolar recycling endosome. Traffic 4, 671–680. [PubMed: 12956870]

Sharma S, Arunachalam PS, Menon M, Ragupathy V, Satya RV, Jebaraj J, Aralaguppe SG, Rao C, Pal S, Saravanan S, et al. (2018). PTAP motif duplication in the p6 Gag protein confers a replication advantage on HIV-1 subtype C. J Biol Chem 293, 11687–11708. [PubMed: 29773649]

Sherer NM, Lehmann MJ, Jimenez-Soto LF, Ingmundson A, Horner SM, Cicchetti G, Allen PG, Pypaert M, Cunningham JM, and Mothes W (2003). Visualization of retroviral replication in living cells reveals budding into multivesicular bodies. Traffic 4, 785–801. [PubMed: 14617360]

Shih SC, Katzmann DJ, Schnell JD, Sutanto M, Emr SD, and Hicke L (2002). Epsins and Vps27p/Hrs contain ubiquitin-binding domains that function in receptor endocytosis. Nat Cell Biol 4, 389–393. [PubMed: 11988742]

Slagsvold T, Aasland R, Hirano S, Bache KG, Raiborg C, Trambaiolo D, Wakatsuki S, and Stenmark H (2005). Eap45 in mammalian ESCRT-II binds ubiquitin via a phosphoinositide-interacting GLUE domain. J Biol Chem 280, 19600–19606. [PubMed: 15755741]

Strack B, Calistri A, Accola MA, Palu G, and Gottlinger HG (2000). A role for ubiquitin ligase recruitment in retrovirus release. Proc Natl Acad Sci U S A 97, 13063–13068. [PubMed: 11087860]

Strack B, Calistri A, and Gottlinger HG (2002). Late assembly domain function can exhibit context dependence and involves ubiquitin residues implicated in endocytosis. Journal of virology 76, 5472–5479. [PubMed: 11991975]

Strickland M, Ehrlich LS, Watanabe S, Khan M, Strub MP, Luan CH, Powell MD, Leis J, Tjandra N, and Carter CA (2017). Tsg101 chaperone function revealed by HIV-1 assembly inhibitors. Nat Commun 8, 1391. [PubMed: 29123089]

Strickland M, Schwieters CD, Göbl C, Opina AC, Strub MP, Swenson RE, Vasalatiy O, and Tjandra N (2016a). Characterizing the magnetic susceptibility tensor of lanthanide-containing polymethylated-DOTA complexes. J Biomol NMR 66, 125–139. [PubMed: 27659040]

Strickland M, Stanley AM, Wang G, Botos I, Schwieters CD, Buchanan SK, Peterkofsky A, and Tjandra N (2016b). Structure of the NPr:EIN(Ntr) Complex: Mechanism for Specificity in Paralogous Phosphotransferase Systems. Structure 24, 2127–2137. [PubMed: 27839951]

Strickland M, and Tjandra N (2018). Residual dipolar coupling for conformational and dynamic studies. In Modern Magnetic Resonance, Webb G, ed. (Cham: Springer).

Sundquist WI, Schubert HL, Kelly BN, Hill GC, Holton JM, and Hill CP (2004). Ubiquitin recognition by the human TSG101 protein. Mol Cell 13, 783–789. [PubMed: 15053872]

Teo H, Veprintsev DB, and Williams RL (2004). Structural insights into endosomal sorting complex required for transport (ESCRT-I) recognition of ubiquitinated proteins. J Biol Chem 279, 28689–28696. [PubMed: 15044434]

Varadan R, Assfalg M, and Fushman D (2005). Using NMR spectroscopy to monitor ubiquitin chain conformation and interactions with ubiquitin-binding domains. Method Enzymol 399, 177–+.

Varadan R, Assfalg M, Haririnia A, Raasi S, Pickart C, and Fushman D (2004). Solution conformation of Lys63-linked di-ubiquitin chain provides clues to functional diversity of polyubiquitin signaling. J Biol Chem 279, 7055–7063. [PubMed: 14645257]

Varadan R, Walker O, Pickart C, and Fushman D (2002). Structural properties of polyubiquitin chains in solution. Journal of molecular biology 324, 637–647. [PubMed: 12460567]

VerPlank L, Bouamr F, LaGrassa TJ, Agresta B, Kikonyogo A, Leis J, and Carter CA (2001). Tsg101, a homologue of ubiquitin-conjugating (E2) enzymes, binds the L domain in HIV type 1 Pr55(Gag). Proc Natl Acad Sci U S A 98, 7724–7729. [PubMed: 11427703]

Vogt VM (2000). Ubiquitin in retrovirus assembly: actor or bystander? Proceedings of the National Academy of Sciences of the United States of America 97, 12945–12947. [PubMed: 11087848]

Votteler J, and Sundquist WI (2013). Virus budding and the ESCRT pathway. Cell Host Microbe 14, 232–241. [PubMed: 24034610]

Vranken WF, Boucher W, Stevens TJ, Fogh RH, Pajon A, Llinas P, Ulrich EL, Markley JL, Ionides J, and Laue ED (2005). The CCPN data model for NMR spectroscopy: Development of a software pipeline. Proteins 59, 687–696. [PubMed: 15815974]

Weeks SD, Grasty KC, Hernandez-Cuebas L, and Loll PJ (2009). Crystal structures of Lys-63-linked tri- and di-ubiquitin reveal a highly extended chain architecture. Proteins 77, 753–759. [PubMed: 19731378]

Weiss ER, Popova E, Yamanaka H, Kim HC, Huibregtse JM, and Gottlinger H (2010). Rescue of HIV-1 release by targeting widely divergent NEDD4-type ubiquitin ligases and isolated catalytic HECT domains to Gag. PLoS Pathog 6, e1001107. [PubMed: 20862313]

Wills JW, and Craven RC (1991). Form, function, and use of retroviral gag proteins. AIDS 5, 639–654. [PubMed: 1883539]

Highlights

- The Tsg101:K63-linked Di-Ub structure is solved by NMR.
- Pseudo contact shifts are used to dock and refine the structure of the complex.
- Lanthanide incorporation into specific Ub could distinguish between two Ub domains.
- Two different conformations of the Di-Ub are required to satisfy the NMR data.

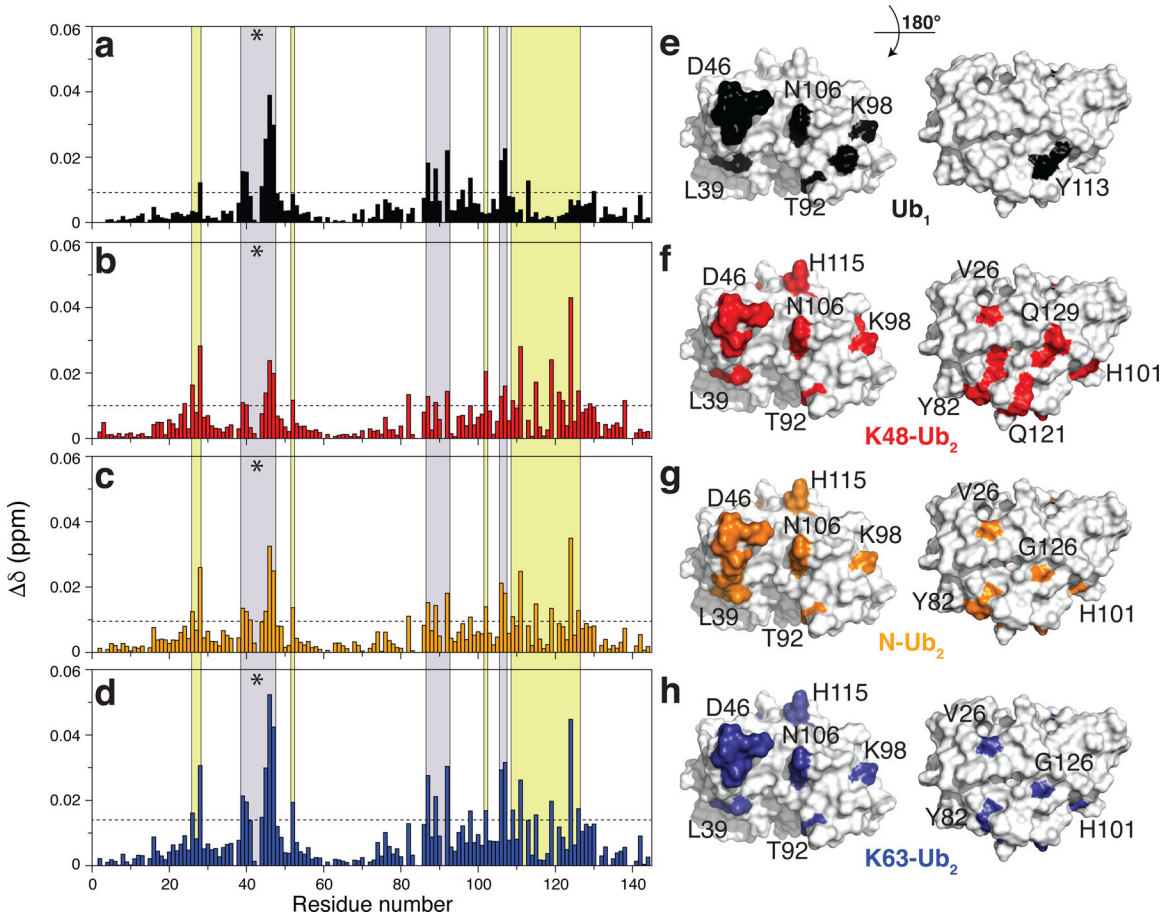

Figure 1.

Tsg101 preferentially binds to K63-Ub_2. **a-d** Residue-specific amide chemical shift perturbations (Δδ) of Tsg101 in the presence of different (poly)ubiquitin molecules. **a**, Ub_1 **b**, K48-Ub_2 **c**, N-Ub_2 **d**, K63-Ub_2. All complexes are in a 1:1 ratio. Large chemical shift perturbations are considered as more than 1.5 standard deviations from zero (above dashed line), or when peaks broaden to zero in the bound form (marked with *). The primary and secondary ubiquitin binding sites of Tsg101 are shaded in grey and yellow, respectively. **e-h** Significant chemical shift perturbations from **a-d** displayed on the surface of Tsg101 (PDB ID: 1S1Q)(Sundquist et al., 2004)). Results for Ub_1 (**a** and **e**) are adapted from Strickland et al. (Strickland et al., 2017) and the figures are shown here for comparison.

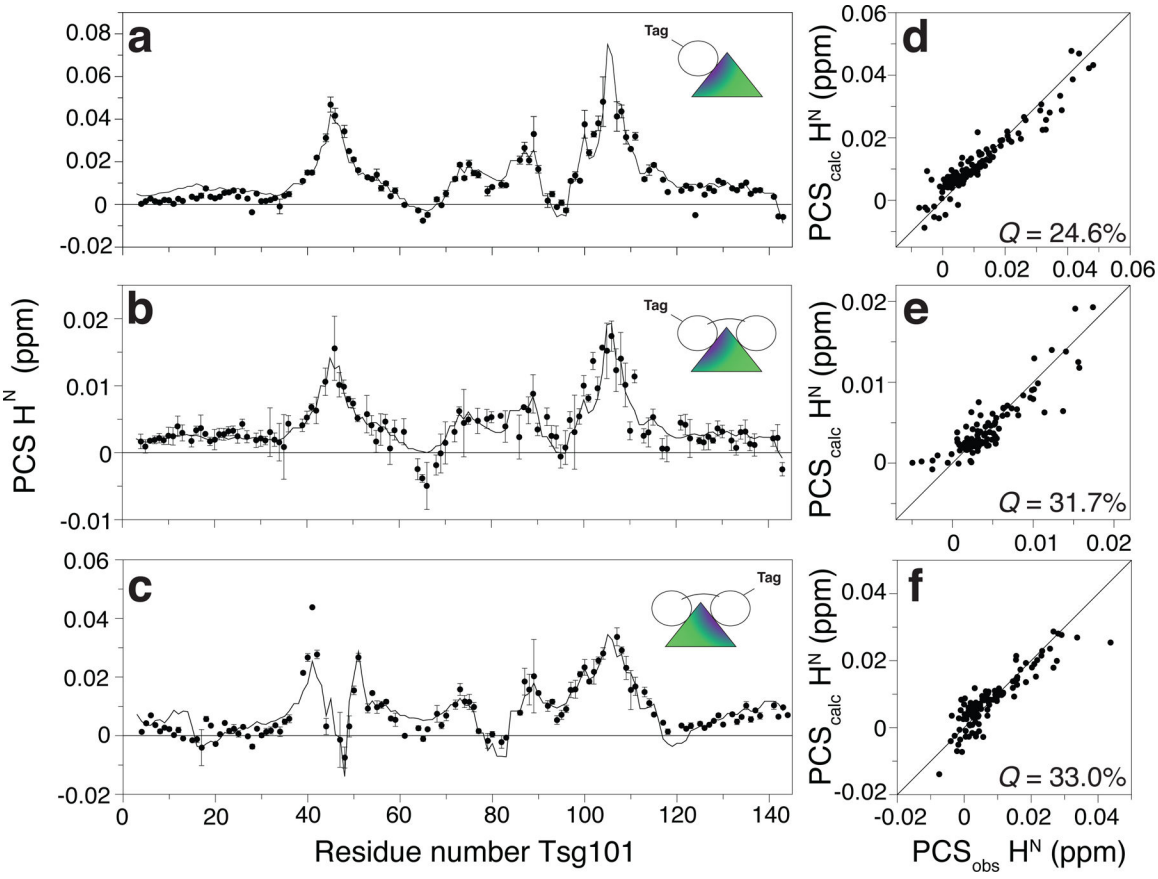

Figure 2.

The distal ubiquitin unit of K63-linked diubiquitin binds in the monoubiquitin site of Tsg101. **a-c** Observed (black circles) and back-calculated (black line) amide proton pseudocontact shifts (PCSs) for ^{15}N-Tsg101 in complex with natural abundance Tm-DOTA-M8-SPy tagged **a**, Ub_1^{T14C} **b**, K63-$Ub_2^{T14C(dist.)}$ or **c**, K63-$Ub_2^{T14C(prox.)}$. **d-f** The observed PCSs (PCS_{obs}) are compared to the calculated PCSs (PCS_{calc}) in scatter plots. The Ub_1 data set is fit to the Tsg101:Ub_1 structure (PDB ID: 1S1Q)(Sundquist et al., 2004) while Ub_2 data sets are fit to the lowest energy Tsg101:K63-Ub_2 complex structure ensemble (n=2) back-calculated in this paper. Q-factors are shown for each scatter plot. Lu-M8-DOTA-SPy tagged proteins were used as the diamagnetic references. Error bars are derived from standard deviations for two sets of experiments (see Methods). The shaded green color in the triangle indicates that Tsg101 is ^{15}N isotopically labeled.

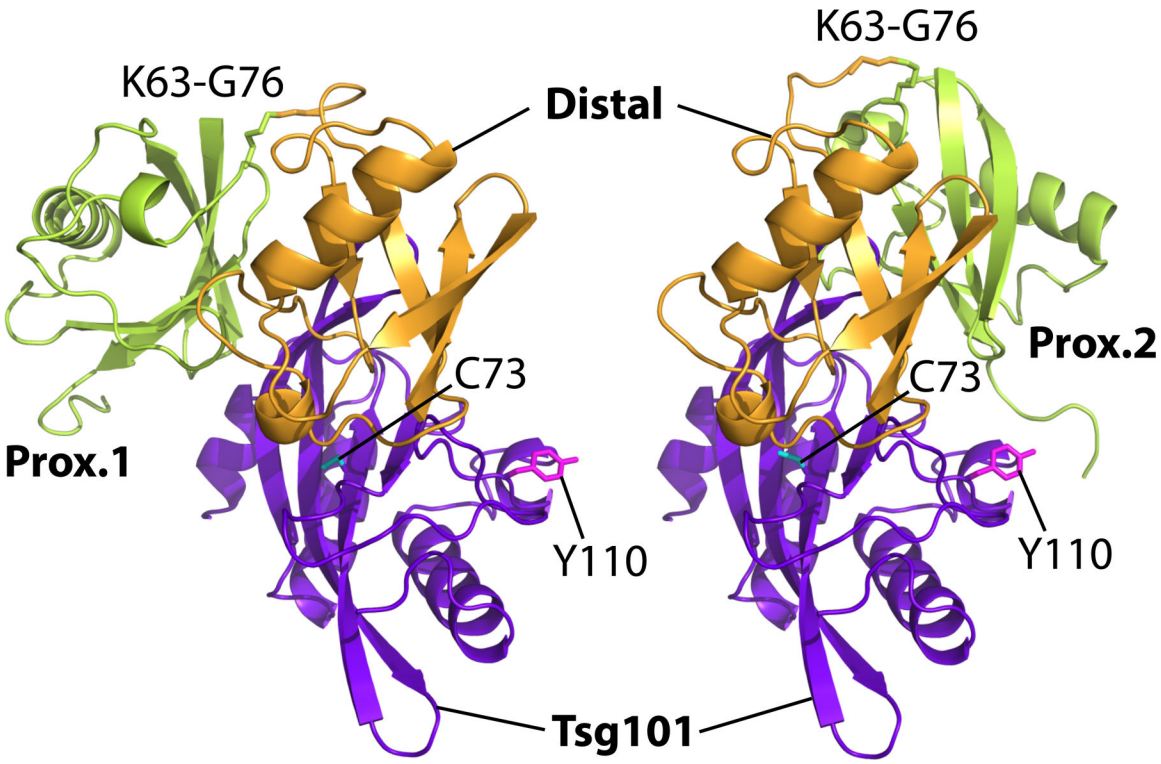

Figure 3.

Structure of the Tsg101:K63-Ub_2 complex. Comparison of the two ensemble members of the lowest energy calculated structures. The distal and proximal Ubs of K63-Ub_2 are shown in orange and green, respectively, while Tsg101 UEV is shown in purple. The potential side-chain interactions of interfacial residues are shown in sticks. Tsg101 residues C73 and Y110 are shown in cyan and magenta, respectively. Figure was rendered using PyMol.

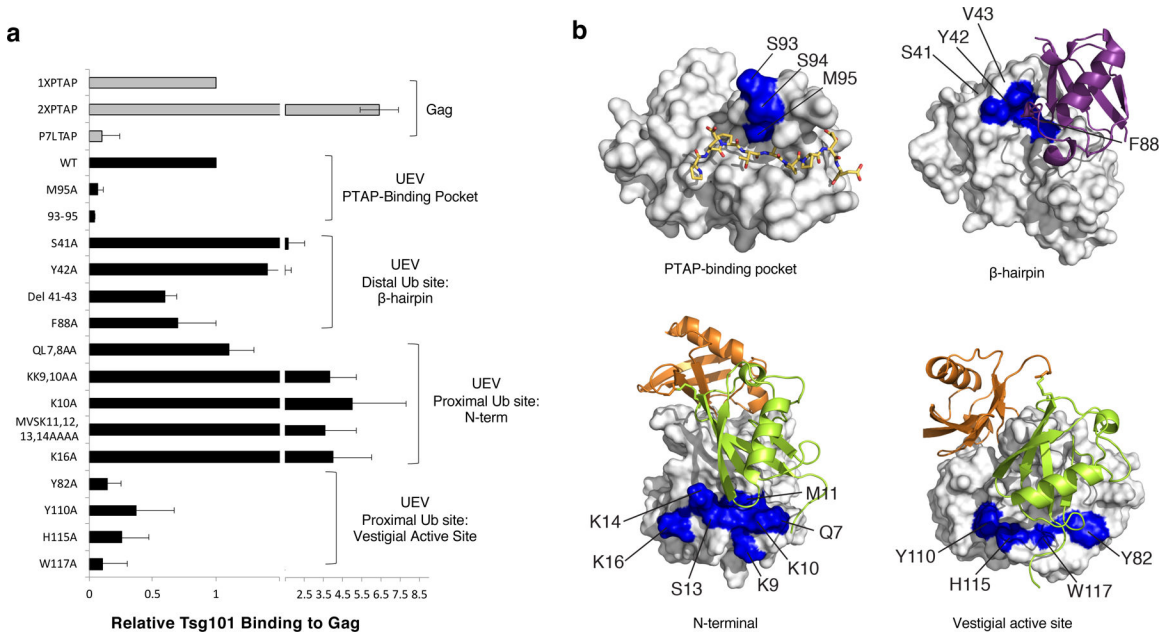

Figure 4.

Mutation of UEV PTAP- and Ub- binding determinants. **a** The impact on Gag-Tsg101 interaction of Ala substitution of the determinants of PTAP- and Ub-binding was tested employing the yeast 2-hybrid assay. Horizontal bars denote assay interaction level as compared to WT Gag-WT Tsg101 binding. Gag and Tsg101 UEV mutations are shown in grey and black, respectively. When analyzed by Student's t-test, Tsg101 mutations were different from wildtype ($p<0.05$) with the exception of S41A, Y42A, F88, and QL7,8AA. **b** Mutations in **a** are highlighted in blue on various complexes of the UEV domain of Tsg101 (white surface). Mutations near the PTAP-binding pocket are shown on the structure of the PTAP:Tsg101 complex (the PTAP peptide is shown in yellow sticks, with nitrogen (blue) and oxygen (red) highlighted, PDB ID: 3OBU (Im et al., 2010)). Mutations in the β-hairpin near the Ub_1 and distal-Ub_2 binding site are shown on the structure of the Ub_1:Tsg101 complex (Ub_1 is in purple, PDB ID: 1S1Q (Sundquist et al., 2004)). Mutations near the two proximal-Ub_2 binding sites are shown on the structure of K63-Ub_2:Tsg101 calculated in this paper [distal Ub (orange), proximal Ub (green)].

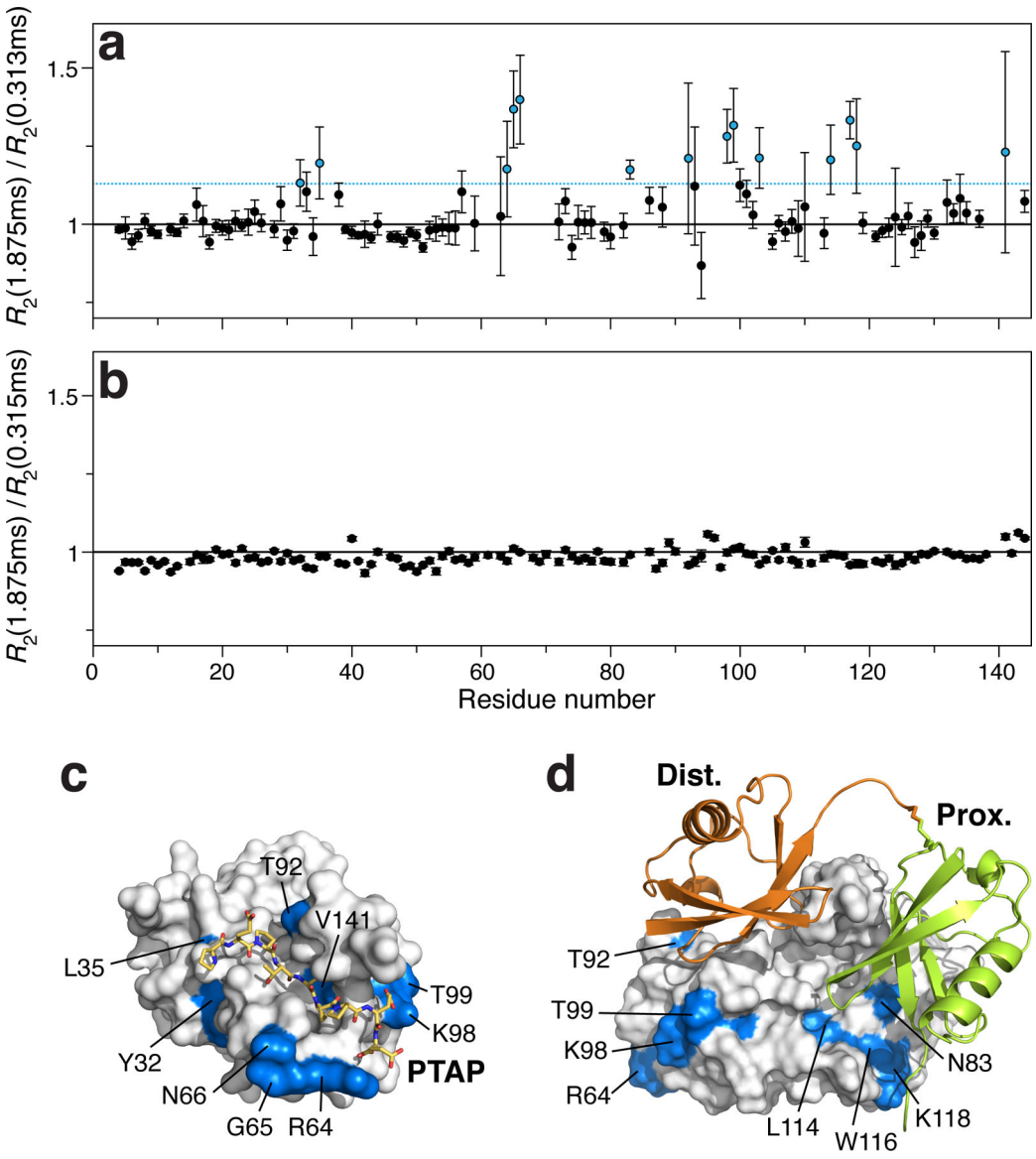

Figure 5.

Effects of microsecond to millisecond dynamics on ^{15}N R_2 CPMG relaxation rates of Tsg101 in the presence and absence of the PTAP peptide. **a** Ratio of Tsg101 R_2 measured at τ_{cp} of 1.875 ms to that at τ_{cp} of 0.313 ms (τ_{cp}) in the presence of PTAP peptide. Significant R_2 enhancement was defined as >1 S.D. from the mean (blue dotted line). Residues with significant R_2 enhancement are highlighted in blue circles. The solid black line represents a ratio of one (no enhancement). Tsg101 and the PTAP peptide were at a 1:1 ratio, both at a concentration of 300 μM. **b** Ratio of Tsg101 R_2 measured at τ_{cp} of 1.875 ms to that at τ_{cp} of 0.315 ms in the absence of PTAP peptide. No residues were observed to have significant R_2 enhancement. The concentration of Tsg101 was 300 μM. Error bars were calculated using error propagation from the noise (see Methods). **c,d** Significant R_2 enhancements from **a** are highlighted in blue on the surface of Tsg101, shown in surface representation. **c** Enhancements are highlighted on the structure of Tsg101 in complex with the PTAP

peptide (yellow sticks, PDB: 3OBU) (Im et al., 2010). **d** Enhancements are highlighted on the structure of Tsg101 in complex with K63-Ub_2 (distal Ub - orange, proximal Ub - green, cartoon) with the proximal Ub in site 2.

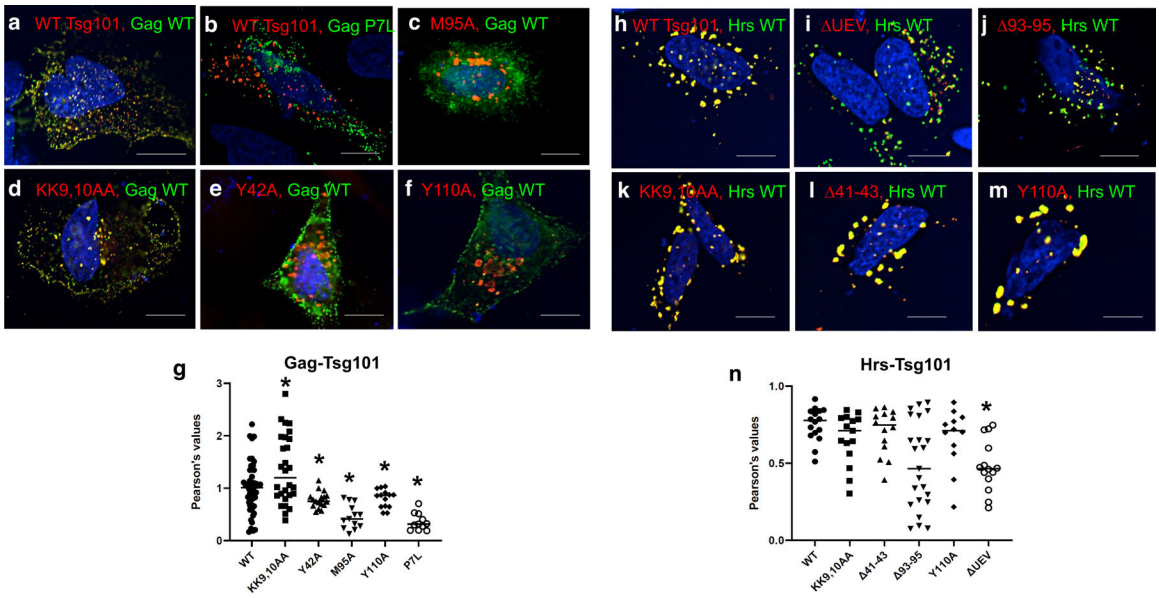

Figure 6.

Determinants of Ub binding in the Tsg101 UEV domain are required for recruitment by HIV-1 Gag but not by the cellular protein Hrs. HIV-1 Gag (panels **a-g**) or Hrs-GFP WT (panels **h-n**) was co-expressed with Myc-tagged Tsg101 WT (panels **a, h**) or mutants (panels **b-f** or panels **i-m**, respectively). Myc-tagged Tsg101 was detected by anti-Myc antibody and Texas Red-tagged secondary antibody. Images were captured on an inverted fluorescence/differential-interference contrast (dic) Zeiss Axiovert 200M fluorescence microscope. HIV-1 WT Gag and WT Hrs recruit Tsg101 to the cell periphery or cell interior (panels **a** and **h**, respectively). Both require determinants of PT/SAP-recognition in the UEV domain (panels **b**, **c** and **i** and **j**, respectively). HIV-1 Gag, but not Hrs, additionally requires determinants of di-Ub-binding located in the UEV α-helix-1, the β-hairpin, and the vestigial active site (compare panels **d-f** to **k-m**). Scale bar equals 10 micrometers. Panels **g** and **n**, Scatter plots of Pearson's correlation coefficients as assessment of recruitment co-localization. Co-localization was assessed for the entire co-transfected cell using Pearson's coefficient of correlation software (NIH Image J, JACoP plugin). Asteriks (*) denote r values that were significantly different from WT control as determined by Tukey's analysis: Panel **g**, ρ = <0.05 (KK9,10AA), <0.01 (Y42A), <0.01 (M95A), <0.05 (Y110A), <0.01 (P7L); panel **n**, ρ = <0.001 (Haynes, 2013).

Table 1.

Structure Calculation Statistics for the Xplor-NIH Structure Determination of Tsg101 in complex with K63-Ub_2 at pH 5.8 and 300 K.

Structural restraints	**K63-Ub_2:Tsg101**
Intermolecular ADRs from CSPs	39
Pseudocontact shifts (^{1}H)	226
Structure Statistics [a]	
RMSD to mean coordinates (Å)[b]	
Backbone (Proximal site 1)	1.2
All heavy atoms (Proximal site 1)	1.7
Backbone (Proximal site 2)	**1.6**
All heavy atoms (Proximal site 2)	**2.0**
Ramachandran plot statistics (%)[b,c]	**K63-Ub $_2$:Tsg101**
Most favored regions	90
Allowed regions	7.8
Disallowed regions	2.1
Deviations from idealized geometry	
Bond lengths (Å)	0.007 ± 0.001
Bond angles (°)	0.740 ± 0.033
Impropers (°)	0.440 ± 0.030
PDB Code: 6UD0	

[a]The structural statistics are displayed in the form of averages and standard deviations for a bundle of the 10 lowest energy structures from a calculation of 100. Each of the structures comprises of two ensemble members.

[b]Determined by PSVS for ordered residues (Bhattacharya et al., 2007).

[c]Calculated using PSVS/Molprobity (Chen et al., 2010).

Abbreviations – Chemical shift perturbations (CSPs), ambiguous distance restraints (ADRs), root mean square deviation (RMSD).

KEY RESOURCES TABLE

REAGENT or RESOURCE	SOURCE	IDENTIFIER
Antibodies		
anti-Myc	Santa Cruz Biotechnology	Cat# sc-40
goat anti-mouse IgG tagged with Texas Red	Thermofisher/ Invitrogen	Cat# T-862
Bacterial and virus strains		
Rosetta™(DE3)pLysS (DE3) Competent Cells	Novagen/Sigma-Aldrich	Cat# 70956
Hela cells	ATCC	ATCC-CCL-2
Chemicals, peptides, and recombinant proteins		
^{15}N Ammonium Chloride	Cambridge Isotope Laboratories	Cat# NLM-467–50
Ace-NFLQSRPEPTAPPEE-$CONH_2$	bioSYNTHESIS	Custom Peptide Synthesis
Ace-NFLQSRPEPTAPPEESW-$CONH_2$	bioSYNTHESIS	Custom Peptide Synthesis
Ampicillin	Sigma-Aldrich	Cat# A9518–25G
Chloramphenicol	Sigma-Aldrich	Cat# C0378–5G
^{13}C D-Glucose	Cambridge Isotope Laboratories	Cat# CLM-1396
d_8-Glycerol	Cambridge Isotope Laboratories	Cat# CDLM-8660
DAPI (4′,6-diamidino-2-phenylindole)	ThermoFisher Scientific	Cat# D1306
Deuterium Oxide	Cambridge Isotope Laboratories	Cat# DLM-4–99.8
β-mecaptoethanol	Sigma-Aldrich	Cat# M6250
Dithiothreitol	Sigma-Aldrich	Cat# D9779
IPTG	Calbiochem	Cat# 420322–25G
Lu- or Tm-M8-DOTA-SPy	Opina *et al.*, 2016	N/A
Roche Complete Protease Inhibitor	Sigma-Aldrich	Cat# 05056489001
Critical commercial assays		
Matchmaker GAL4 Yeast Two Hybrid β-galactosidase assay	Clontech Laboratories, Inc.	Cat# 630489
QuikChange II XL site-directed mutagenesis kit	Agilent Technologies	Cat# 200522–5
Deposited data		
Protein structures	Sundquist *et al.*, 2004	PDB: 1S1Q
Protein structures	Weeks *et al.*, 2009	PDB: 3H7P
Protein structures	Maltsev *et al.*, 2014	PDB: 2MJB
Protein structures	This paper	PDB: 6UD0
NMR structural restraints	This paper	PDB: 6UD0

REAGENT or RESOURCE	SOURCE	IDENTIFIER
NMR chemical shifts	This paper	BMRB: 30675
Experimental models: Cell lines		
Saccharomyces cerevisiae strain Y190	ATCC	Y190
Recombinant DNA		
pET-21a di-ubiquitin	This study	N/A
pET-21a mono-ubiquitin	Opina *et al.*,2016	N/A
pET-28b N-terminally His_6-tagged Tsg101 UEV domain (residues 2–145)	Strickland *et al.*, 2017	N/A
pCMV-Gag-EGFP	Goff *et al.*, 2003	N/A
pLLEXP1-hTsg101-Myc	Goff *et al.*, 2003	N/A
pAcGFP1-N1-mHRS	This paper	N/A
pGAD424-Tsg101	This paper	N/A
pGBT9-HIV-1 Gag	This paper	N/A
Software and algorithms		
CCPN Version 2	Vranken *et al.*, 2005	https://www.ccpn.ac.uk/v2-software
NIH Image J, JACoP plugin	Bolte and Cordelieres, 2006	https://imagejdocu.tudor.lu/doku.php?id=plugin:analysis:jacop_2.0:just_another_colocalization_plugin:start
NMRPipe	Delaglio *et al.*, 1995	https://spin.niddk.nih.gov/bax/software/NMRPipe/Install/
NMRFAM-Sparky v 1.414	Lee *et al.*, 2014	https://nmrfam.wisc.edu/nmrfam-sparky-distribution/
Protein Structure Validation Suite	Bhattacharya *et al.*, 2007	https://montelionelab.chem.rpi.edu/PSVS/
Pymol	Schrodinger, 2015	http://pymol.org
Topspin 3.0	Bruker Corporation	https://www.bruker.com/products/mr/nmr/nmr-software/software/topspin
XIPP	Garrett et al., 2020	https://spin.niddk.nih.gov/dgarrett/Xipp/xipp.html
XPLOR NIH	Schwieters *et al.*, 2006; Schwieters *et al.*, 2003	https://nmr.cit.nih.gov/xplor-nih/
Other		
Amicon Ultracel 3000 MWCO	Millipore	Cat# UFC900396
5mm Shigemi Tube, 8 mm Bottom	Wilmad-LabGlass	Cat# BMS-005B
HiTrap Q HP column, 5mL	GE Healthcare	Cat# GE17-1154-01
HiTrap SP HP column, 5mL	GE Healthcare	Cat# GE17-1152-01
HiLoad 26/60 Superdex 75 prep grade	GE Healthcare	Cat# GE28-9893-36